



Dipl.-Ing. Ulrich Rößl, BSc

# Freeze-Thaw Behavior of Pharmaceutical Proteins

The Effects of Bulk-Scale Freezing and Thawing Operations on the  
Stability of Proteins

DISSERTATION

zur Erlangung des akademischen Grades

Doktor der technischen Wissenschaften

eingereicht an der

**Technischen Universität Graz**

Betreuer

Univ.-Prof. Dipl.-Ing. Dr.techn. Bernd Nidetzky

Institut für Biotechnologie und Bioprozesstechnik

Graz, Juni 2014



# EIDESSTATTLICHE ERKLÄRUNG

## AFFIDAVIT

Ich erkläre an Eides statt, dass ich die vorliegende Arbeit selbstständig verfasst, andere als die angegebenen Quellen/Hilfsmittel nicht benutzt, und die den benutzten Quellen wörtlich und inhaltlich entnommenen Stellen als solche kenntlich gemacht habe. Das in TUGRAZonline hochgeladene Textdokument ist mit der vorliegenden Dissertation identisch.

*I declare that I have authored this thesis independently, that I have not used other than the declared sources/resources, and that I have explicitly indicated all material which has been quoted either literally or by content from the sources used. The text document uploaded to TUGRAZonline is identical to the present doctoral dissertation.*

---

Datum / Date

---

Unterschrift / Signature

*Für Karoline*

## Abstract

Freezing is a common means for storing bulk volumes of pharmaceutical protein solutions. Process development at industrial scale is usually expensive. Results from stability testing at small mL-scale however often cannot be transferred to higher volumes.

In this doctoral thesis I studied the stability of pharmaceutical proteins in freezing and thawing processes at laboratory- and pilot-scale. For that purpose, two stainless steel freeze containers with reduced volumes, 200 mL and 700 mL, were designed and constructed in collaboration with Zeta Biopharma. Characteristic bulk scale phenomena, such as cryoconcentration and low degrees of supercooling, were observed at these intermediate scales. A computational fluid dynamic simulation, established at the RCPE, was developed and validated using the 200 mL container. Predictions of heat and mass transfer during freezing processes facilitate the design of new container sizes and geometries. The impact of processing parameters on quality attributes of L-lactic dehydrogenase (LDH) was investigated in the 700 mL model. Especially variation of storage temperature impaired LDH stability with up to complete inactivation at low temperatures. Precipitation of buffer components upon freezing caused LDH inactivation due to increased surface exposure and/or extreme shift of pH in ice.

A method was developed for in-situ monitoring of conformational protein stability in the frozen state. Employing Raman spectroscopy it is possible to quantitatively estimate secondary structural elements of frozen proteins. This method can be used in the presence of common stabilizers and provides almost real-time information about protein conformation during freeze and thaw processing in stainless steel containers.

## Zusammenfassung

Einfrieren ist eine gängige Methode um große Volumina pharmazeutischer Proteinlösungen zu lagern. Die Entwicklung von Einfrier- und Auftauprozessen im industriellen Maßstab ist dabei häufig sehr kostspielig. Resultate von Stabilitätsstudien im kleinen mL-Maßstab sind aber meist nicht auf größere Volumina übertragbar.

Im Rahmen meiner Dissertation untersuchte ich die Stabilität von pharmazeutischen Proteinen während Einfrier- und Auftauprozessen im Labor- und Pilot-Maßstab. In Zusammenarbeit mit Zeta Biopharma wurden zu diesem Zweck zwei Gefriercontainer aus rostfreiem Stahl entworfen und gefertigt. Ihre Volumina betragen 200 mL bzw. 700 mL.

Charakteristika von großtechnischen Prozessen, wie etwa Kryokonzentrierung und geringe Unterkühlung, konnten im reduzierten Maßstab beobachtet werden. Eine numerische Strömungsmechanik-Simulation (computational fluid dynamic, CFD), erstellt am RCPE, wurde anhand des 200 mL-Containers entwickelt und validiert. Vorhersagen über Wärme- und Massentransfer während Einfrierprozessen erleichtern das Design von neuartigen Containergrößen und -geometrien.

Der Einfluss von Prozessparametern auf Qualitätsattribute von L-Laktatdehydrogenase (LDH) wurde im 700 mL-Modell untersucht. Insbesondere durch Variationen der Lagertemperatur wurde die Stabilität von LDH deutlich beeinträchtigt. Bei niedrigen Temperaturen wurde zum Teil völlige Inaktivierung des Enzyms festgestellt. Präzipitation von Pufferbestandteilen beim Einfrieren führte zur LDH-Inaktivierung aufgrund von erhöhtem Oberflächenstress und/oder extremer pH-Verschiebung im Eis.

Eine Methode zur in-situ-Überwachung von konformationeller Proteinstabilität im gefrorenen Zustand wurde zudem entwickelt. Mithilfe von Raman-Spektroskopie ist eine quantitative Abschätzung von Sekundärstrukturelementen gefrorener Proteine möglich. Diese Methode kann in Gegenwart einiger verbreiteter Stabilisatoren angewandt werden und liefert dabei nahezu in Echtzeit Informationen über Proteinkonformation während Einfrier- und Auftauprozessen sowie Lagerung im gefrorenen Zustand.

## Acknowledgements

My sincere thanks and appreciation for a marvelous supervision go to Prof. Bernd Nidetzky. His mentoring was both guiding and stimulating, and he left me enough room for my own ideas and my personal development.

I feel highly grateful to Stefan Leitgeb for his never-ending support. I hope he will find his way back into biotechnology, soon.

My highest thanks go to my wife and my family for their support and patience. Thank you for backing me up during strenuous times.

Special thanks to Stefan Spörk, Ewald Rössl, Thomas Stoisser, Lisa Uhlmann, Patricia Wildberger, Bernd Wolfgruber and the Internet.

# Contents

1	Extended Abstract .....	1
2	Characterization of a Laboratory-Scale Container for Freezing Protein Solutions with Detailed Evaluation of a Freezing Process Simulation.....	8
3	Visualizing Cryoconcentration of Proteins in a Laboratory-Scale Freeze Container.....	19
4	The Impact of Freeze-And-Thaw Processing Conditions on Protein Stability: A Pilot-Scale Study of L-Lactic Dehydrogenase.....	29
5	In-Situ Protein Secondary Structure Determination in Ice: Raman Spectroscopy-Based Process Analytical Tool for Frozen Storage of Biopharmaceuticals.....	53

# 1 Extended Abstract

Protein-based biopharmaceuticals are one of the greatest trends in pharmaceutical market reports from recent years. In 2009, global market value of recombinant monoclonal antibodies and other therapeutic proteins reached \$99 billion,<sup>1</sup> further increasing to \$110 billion in 2012.<sup>2</sup> It represents the fastest growing segment of the worldwide \$600 billion pharmaceutical market.<sup>1</sup> Fields of application for protein biopharmaceuticals are broad. Various types of cancerous and inflammatory diseases are treated with recombinant antibody products. Other recombinant protein preparations are applied against diabetes mellitus, myocardial infarction, hemophilia, hepatitis C, multiple sclerosis and hematopoietic deficiencies. Also components for numerous vaccines represent a major part of protein pharmaceuticals.<sup>1</sup> Accordingly, manufactured volumes of biopharmaceuticals are large. In 2012, global cell culture capacity accounted for 3.1 million liters and is expected to grow to 4.0 million liters by 2018.<sup>3</sup>

The enormous volumes produced for that globalized market pose a challenge, not only for worldwide logistics, but also for coordination of operations in production, downstream processing and fill & finish. Manufacturing still occurs discontinuously for most biopharmaceuticals, and the volume of pharmaceutical protein batches often don't match momentary demands of the market or the subsequent processing step.

Freezing of biopharmaceutical protein solutions at bulk scales of up to 300 liters represents a convenient solution for these issues. Shelf life between processing operations can be extended by frozen storage. Also shipment in the frozen state offers advantages over liquid shipment. Temperature can be controlled more effectively, and agitation stresses are avoided. Therefore, it does not surprise that almost half of commercial biopharmaceuticals are estimated to be stored frozen.<sup>4</sup>

Usually, bulk volumes of protein solutions are frozen either in disposable plastic vessels, such as bottles or bags, or in stainless steel containers. While bottles are primarily subjected to uncontrolled shelf-freezing, bag systems for controlled freezing of volumes of up to 16 liters are available, such as for the Celsius™-Pak-System by Sartorius. These systems offer convenient handling due to simplified containment, and they are claimed to facilitate freezing and thawing (F/T) process characterization and scale-up.<sup>5</sup> Yet unresolved and hardly predictable risks related to the use of disposable F/T container

vessels comprise product contamination with leachables and extractables, especially at deep freezing temperatures.<sup>6,7</sup> Here, the use of stainless steel containers can be advisable. Also, higher storage volumes of 300 liters can be reached with stainless steel containers, e.g. with the FreezeContainer™ system by Zeta Biopharma.

Despite of the high relevance of F/T and frozen storage as unit operations in biopharmaceutical manufacturing industry, the quantity of published research work in the field of industrial-scale freezing is low. Only few, yet excellent, publications review relevant research on bulk-scale freezing of proteins.<sup>4,8,9</sup> The vast majority of investigations of F/T effects on protein stability were conducted at mL-scale. There, experimental conditions do not reflect heat- and mass transfer conditions of larger scales and the complications related. Experiments at bulk scales are often too expensive for academic research, while a lot of empirical knowledge remains undisclosed by the industry.<sup>4</sup> Beyond dispute, however, is the fact that proteins react very differently upon freezing stresses. Freezing process characterization has to be performed for every protein, individually, as different types of stresses take effect during F/T. Low temperature per se can cause protein unfolding.<sup>10,11</sup> The effect known as cold denaturation is defined as reversible upon re-heating. Thus, cold denaturation alone is usually not responsible for protein destabilization in ice. It could however render the protein more susceptible to denaturation through other freeze-related stress factors.<sup>9</sup> One of them is surface stress derived from water crystallization. Particularly, proteins which are sensitive to interfacial stresses often appear likewise susceptible to denaturation due to freezing.<sup>12</sup> Also, precipitation or crystallization of co-solutes can promote surface-induced protein unfolding in the frozen state, as shown for sorbitol and trehalose.<sup>13,14</sup> Precipitation of buffer components during the cooling phase can furthermore lead to substantial pH-shifts.<sup>15,16</sup> Sodium phosphate buffer is well known for such a behavior,<sup>17</sup> and its consequences on protein stability were documented in several occasions.<sup>18,19</sup> Issues connected with poor solubility of solutes can be aggravated at higher scales through cryoconcentration effects. As solutes are expelled from the growing ice front they concentrate in the last points to freeze. Steep concentration gradients can form, which promote phase separation. For proteins undergoing cryoconcentration, concomitant desiccation could impair protein stability when water is removed from the protein's hydration shell during freezing.<sup>9,20</sup>

To a certain extent, the impact of these factors on protein stability can be limited. Usually, this is done via adaptations in formulation compositions. Compounds that are prone to precipitate or crystallize in the frozen state can be avoided. The choice of the appropriate buffer prevents destabilization due to pH-shifts. As storage below  $T_g'$  (glass transition temperature of the freeze concentrated matrix) is

advisable for most proteins, excipients that elevate  $T_g'$  can be added.<sup>4</sup> Usually, high protein concentrations during frozen storage yield higher stabilities than diluted solutions.<sup>9</sup>

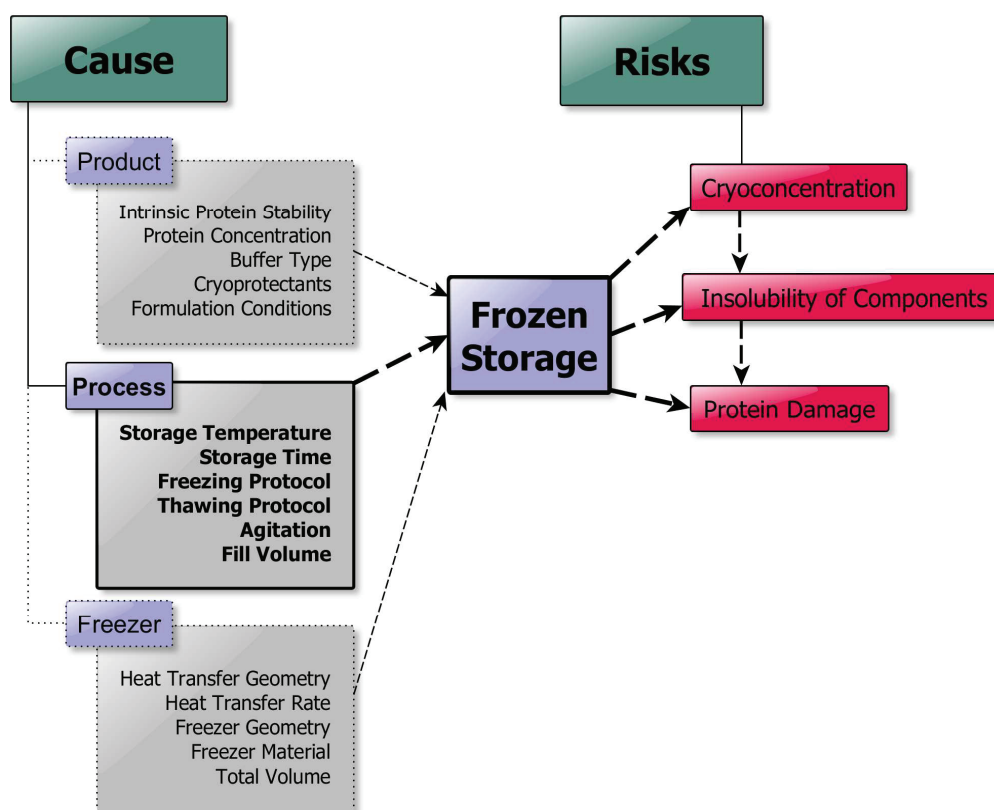


**Figure 1: Several parameters deriving from product-, process-, or freezer characteristics can impair protein stability during freezing and frozen storage. Cryoconcentration, insolubility of (co-)solutes and direct protein damage by the ice surface can be the result of suboptimal process design, depending on the intrinsic stability of the stored protein towards different types of stresses.**

Less is known about the impact of process conditions on frozen protein stability. As mentioned above, protein solutions are mostly stored below  $T_g'$ , since the reduced diffusive mobility in the glassy matrix hinders protein aggregation.<sup>9</sup> Other processing parameters such as cooling/heating rates can only be considered with regard to the used freezing setup. Heat transfer rates (HTR), geometry, container material, and frozen volume are ultimately related to processing parameters, which are thus hardly comparable between the systems. Figure 1 comprises parameters which can impair the stability of proteins frozen and stored in the frozen state.

The actual impact of single parameters on protein stability has to be determined for each protein preparation anew. Process characterization and optimization can thus get very time-consuming and expensive, given the large volumes of high-value product processed. F/T process characterization at

intermediate scales would lower these efforts. At the same time, special features found in the industrial bulk scales remained observable, such as cryoconcentration, low HTRs, little supercooling etc.

In this thesis, special emphasis is therefore placed on laboratory- and pilot-scale freeze containers and their application for F/T process development, characterization, and optimization. The first part focuses on the characterization of a freezing process in a 200 mL laboratory-scale container. I investigated temperature progression, macroscopic cryoconcentration, and stability of the model protein L-lactic dehydrogenase (LDH) in multiple sampling positions of the frozen bulk. In addition, I compared temperature, ice front progression, and protein concentration with results from a computational fluid dynamic (CFD) model developed at the RCPE. This model could facilitate the design of new container sizes and geometries by predicting freezing kinetics and protein distribution in ice.

In the second part I present a method for the visualization of microscopic cryoconcentration in a 200 mL lab scale freeze container. Employing confocal laser scanning microscopy of ice core samples the impact of sampling position and solidification rate can be evaluated.

The third part of this thesis elucidates the impact of various process parameters on a pilot-scale F/T operation of LDH-solutions with a volume of up to 700 mL. Furthermore, the mechanism of LDH inactivation in the respective system was determined. I demonstrate that the 700 mL freeze container represents a QbD-compliant (Quality by Design) tool for efficient development of F/T processes at a reduced scale.

For the last part of my thesis I developed a method for in-situ monitoring of secondary protein structure in the liquid and the frozen state. Using Raman spectroscopy a quantitative estimation of the content of  $\alpha$ -helix,  $\beta$ -sheets, and other secondary structure elements is possible from frozen protein solutions. By comparison with qualitative data from literature I show that the method delivers valid results and that it provides valuable structural information under various conditions.

This thesis covers some essential aspects of bulk scale freezing of protein pharmaceuticals. The findings will contribute to a deeper understanding of an important unit operation, that is yet underrepresented in literature. Hence, still numerous issues need to be investigated for a comprehensive knowledge of the basic relevant factors influencing protein stability. E.g. nature and magnitude of interactions between proteins and ice crystal surfaces are still largely unclear. Deeper investigations could increase our knowledge about cryoconcentration effects, their impact on protein stability, as well as their predictability with molecular dynamic or CFD simulations. However, considering the development of this project and the excellent progress that was possible in this environment, I feel confident that this thesis will one day be considered as initial step for a long-lasting

and successful period of research and development in the field of protein freezing at the RCPE and the Graz University of Technology.

## References

1. Walsh G. 2010. Biopharmaceutical benchmarks 2010. *Nat Biotechnol.* 28:917–924.
2. Rader RA. 2012. Fda biopharmaceutical product approvals and trends in 2012. *Bioprocess Int.* 11:18–27.
3. Berner I, Dexter S, Galliher P. 2013. Global evolution of biomanufacturing. *Bioprocess Int.* 11:12–17.
4. Singh S, Kolhe P, Wang W, Nema S. 2009. Large-scale freezing of biologics; A practitioner's review. Part one: Fundamental aspects. *Bioprocess Int.* 7:32–44.
5. Radmanovic N, Serno T. 2013. Understanding the freezing of biopharmaceuticals: First principle modeling of the process and evaluation of its effect on product quality. *J Pharm Sci.* 102:2495–2507.
6. Bezawada A, Thompson M, Cui W. 2011. Use of blast freezers in vaccine manufacture. *Bioprocess Int.* 9:42–51.
7. Bee J, Randolph T. 2011. Effects of surfaces and leachables on the stability of biopharmaceuticals. *J Pharm Sci.* 100:4158–4170.
8. Singh SK, Kolhe P, Wang W, Nema S. 2009. Large-scale freezing of biologics; A practitioner's review. Part two: Practical advice. *Bioprocess Int.* 7:34–42.
9. Singh SK, Nema S. 2010. Freezing and thawing of protein solutions. In Jameel F, Hershenson S, editors. *Formul Process Dev Strateg Manuf Biopharm.* John Wiley & Sons. 625–675.
10. Privalov PL. 1990. Cold denaturation of proteins. *Crit Rev Biochem Mol Biol.* 25:281–306.
11. Franks F. 1995. Protein destabilization at low temperatures. *Adv Protein Chem.* 46:105–139.
12. Chang BS, Kendrick BS, Carpenter JF. 1996. Surface-induced denaturation of proteins during freezing and its inhibition by surfactants. *J Pharm Sci.* 85:1325–1330.
13. Piedmonte DM, Summers C, McAuley A, Karamujic L, Ratnaswamy G. 2007. Sorbitol crystallization can lead to protein aggregation in frozen protein formulations. *Pharm Res.* 24:136–146.
14. Singh SK, Kolhe P, Mehta AP, Chico SC, Lary AL, Huang M. 2011. Frozen state storage instability of a monoclonal antibody: Aggregation as a consequence of trehalose crystallization and protein unfolding. *Pharm Res.* 28:873–885.
15. Sundaramurthi P, Shalaev E, Suryanarayanan R. 2010. “pH swing” in frozen solutions—Consequence of sequential crystallization of buffer components. *J Phys Chem Lett.* 1:265–268.

16. Kolhe P, Amend E, Singh SK. 2009. Impact of freezing on pH of buffered solutions and consequences for monoclonal antibody aggregation. *Biotechnol Prog.* 26:727–733.
17. Van Den Berg L, Dyson R. 1959. Effect of freezing on the pH and composition of sodium and potassium phosphate solutions: the reciprocal system  $\text{KH}_2\text{PO}_4\text{-Na}_2\text{HPO}_4\text{-H}_2\text{O}$ . *Arch Biochem Biophys.* 81:319–329.
18. Pikal-Cleland K. 2000. Protein denaturation during freezing and thawing in phosphate buffer systems: Monomeric and tetrameric  $\beta$ -galactosidase. *Arch Biochem Biophys.* 384:398–406.
19. Pikal-Cleland KA, Cleland JL, Anchordoquy TJ, Carpenter JF. 2002. Effect of glycine on pH changes and protein stability during freeze–thawing in phosphate buffer systems. *J Pharm Sci.* 91:1969–1979.
20. Anchordoquy TJ, Carpenter JF. 1996. Polymers protect lactate dehydrogenase during freeze-drying by inhibiting dissociation in the frozen state. *Arch Biochem Biophys.* 332:231–238.

## **2 Characterization of a Laboratory-Scale Container for Freezing Protein Solutions with Detailed Evaluation of a Freezing Process Simulation**

# Characterization of a Laboratory-Scale Container for Freezing Protein Solutions with Detailed Evaluation of a Freezing Process Simulation

ULRICH ROESSL,<sup>1,2</sup> DALIBOR JAJCEVIC,<sup>1</sup> STEFAN LEITGEB,<sup>1</sup> JOHANNES G. KHINAST,<sup>1,3</sup> BERND NIDETZKY<sup>2</sup>

<sup>1</sup>Research Center Pharmaceutical Engineering, Graz, Austria

<sup>2</sup>Institute of Biotechnology and Biochemical Engineering, Graz University of Technology, Graz, Austria

<sup>3</sup>Institute of Process and Particle Engineering, Graz University of Technology, Graz, Austria

Received 10 September 2013; revised 13 November 2013; accepted 20 November 2013

Published online 13 December 2013 in Wiley Online Library (wileyonlinelibrary.com). DOI 10.1002/jps.23814

**ABSTRACT:** A 300-mL stainless steel freeze container was constructed to enable QbD (Quality by Design)-compliant investigations and the optimization of freezing and thawing (F/T) processes of protein pharmaceuticals at moderate volumes. A characterization of the freezing performance was conducted with respect to freezing kinetics, temperature profiling, cryoconcentration, and stability of the frozen protein. Computational fluid dynamic (CFD) simulations of temperature and phase transition were established to facilitate process scaling and process analytics as well as customization of future freeze containers. Protein cryoconcentration was determined from ice-core samples using bovine serum albumin. Activity, aggregation, and structural perturbation were studied in frozen rabbit muscle l-lactic dehydrogenase (LDH) solution. CFD simulations provided good qualitative and quantitative agreement with highly resolved experimental measurements of temperature and phase transition, allowing also the estimation of spatial cryoconcentration patterns. LDH exhibited stability against freezing in the laboratory-scale system, suggesting a protective effect of cryoconcentration at certain conditions. The combination of the laboratory-scale freeze container with accurate CFD modeling will allow deeper investigations of F/T processes at advanced scale and thus represents an important step towards a better process understanding. © 2013 Wiley Periodicals, Inc. and the American Pharmacists Association *J Pharm Sci* 103:417–426, 2014

**Keywords:** computational fluid dynamics; enzymes; fluorescence spectroscopy; freezing/thawing; HPLC; protein aggregation; protein folding; protein stability; thermal analysis

## INTRODUCTION

Freezing is a common and convenient means of storing pharmaceutical protein solutions at industrial scale. It serves to increase flexibility of the manufacturing process with respect to short- or medium-term market demands. The risk of inactivation and microbial contamination is lowered and transportation of the frozen bulk is facilitated compared with the liquid state.<sup>1</sup> Despite its seeming simplicity, freezing and thawing (F/T) can form a critical unit process. Losses of valuable protein because of the aggregation or inactivation can add up to 60%, even in few milliliter volumes.<sup>2,3</sup> Cryoconcentration and surface exposure are even more pronounced when bulk volumes in the range of some 100 mL to several 100 L are frozen.<sup>4</sup> Bottles or plastic bags are frequently used for storing at around liter scale in simple freezers operated at constant temperatures. Here, process surveillance and control are largely neglected. Integrated bulk freezing systems (Zeta FreezeContainer<sup>TM</sup>, Sartorius CryoVessel<sup>TM</sup>) on the contrary comprise those factors and offer wide influence on heat transfer, temperature, and even mixing.<sup>5</sup> Monitoring of temperature facilitates quality assurance and optimization of storage conditions. Optimal condi-

tions for freezing, storage, and thawing vary depending on the characteristics of the protein, buffer, excipients, and their concentrations by influencing  $T_M$ ,  $T_G$ , pH, solubility, and osmotic pressure.<sup>1</sup> Cooling and heating rates have effects on the ice surface exposure of proteins via the extent of undercooling, nucleation, and supersaturation.<sup>6</sup>

All these factors are crucial for protein freezing and complicate the optimization of the process for large volumes. Results of existing studies on protein F/T in small milliliter scale<sup>7–9</sup> cannot be simply extrapolated to bulk volume conditions. For the latter, experimental studies are scarce and usually expensive.<sup>10–12</sup>

Medium-scale freezing containers can close the gap between simple small-volume F/T experiments lacking relevance for bulk storage and costly testing at original scale.<sup>13,14</sup>

However, the impact of the process scale on product quality is not well understood. Especially, the consequences of cryoconcentration such as pH shift and solute precipitation/crystallization might severely impair protein stability, and they vary considerably with the bulk volume. Although laboratory-scale freezers would certainly increase the efficiency of process optimization, only a deeper process understanding can lead to reliable scalability and adaption to demands of pharmaceutical producers. Predictability of temperatures, phase transition, and cryoconcentration would enable the manufacturing of custom-made cryovessels, allowing the variation of geometry, heat transfer rate, and volume. Even the placement of different analytical probes (e.g., temperature and pH) or other installations (e.g., for mixing and filling/emptying) could then occur based on the predictions of last freezing spots, hot/cold

**Abbreviations used:** ANS, 8-anilino-1-naphthalenesulfonic acid; BSA, bovine serum albumin; F/T, freezing and thawing; HTC, heat transfer coefficient; LDH, lactic dehydrogenase; NTU, nephelometric turbidity units; QbD, Quality by Design; SE-HPLC, size-exclusion high-pressure liquid chromatography.

**Correspondence to:** Bernd Nidetzky (Telephone: +43 (316) 873-8400; Fax: +43 (316) 873-8434; E-mail: bernd.nidetzky@tugraz.at)

*Journal of Pharmaceutical Sciences*, Vol. 103, 417–426 (2014)

© 2013 Wiley Periodicals, Inc. and the American Pharmacists Association

spots, or cryoconcentrated regions. The recent advent of Quality by Design (QbD) in pharmaceutical industry is an additional driving force toward the enhancement of process understanding. Process scaling, simulation, and characterization represent fundamental QbD principles that can be realized by the combination of a laboratory-scale freeze container together with functional numerical simulations.

Therefore, a 300-mL stainless steel freeze container was designed and constructed in close collaboration with Zeta Biopharma, and a method for the simulation of F/T processes utilizing computational fluid dynamics (CFD) was developed. The established model will allow for the prediction of temperature and F/T-process-related phase transition and thereby enable *in silico* process characterization, but also the optimization of future container and process designs. The use of seven temperature probes inside of the laboratory-scale freeze container, together with infrared thermography, enables the calibration and evaluation of simulation results at a resolution not reached in comparable studies.<sup>13–15</sup>

Bovine serum albumin and L-lactic dehydrogenase (LDH) from rabbit muscle were used as model proteins to investigate the characteristics of the system when freezing protein solutions. LDH stability was monitored measuring catalytic activity, tryptophane, and 8-anilino-1-naphthalenesulfonic acid (ANS) fluorescence. Aggregation was measured with size-exclusion HPLC (SE-HPLC) and turbidimetry. Cryoconcentration of buffer components was also assessed for the buffer anion phosphate.

## MATERIALS AND METHODS

### Materials

Lyophilized LDH from rabbit muscle was from Merck Chemicals (Darmstadt, Germany). Lyophilized BSA and ANS were from Sigma–Aldrich (St. Louis, Missouri). Unless mentioned, all other chemicals and reagents used were from Carl Roth GmbH + Company KG (Karlsruhe, Germany).

Various sizes of Vivaspin ultrafiltration columns (MWCO 10 kDa) from GE Healthcare (Little Chalfont, UK) were used for buffer exchange.

### Sample Preparation

Lyophilized proteins were dissolved in 50 mM potassium phosphate buffer, pH 7.5 to yield a concentration of 1 mg/mL. After the removal of impurities with spin columns and 0.45  $\mu\text{m}$  filtration, solutions were diluted to 100  $\mu\text{g}/\text{mL}$ . A total volume of 200 mL was subjected to freezing in the laboratory-scale freeze container.

### Freezer Design

The Zeta laboratory-scale freeze container enables investigation of bulk freezing effects in a moderate volume with online monitoring of the bulk temperature at seven positions (Fig. 1). Material properties of the stainless steel vessel (AISI316L—1.4435/1.4404,  $R_a < 0.8 \mu\text{m}$ ) are the same as in the commercial 300 L FreezeContainer™ by Zeta Biopharma GmbH (Lieboch, Austria). The jacket is cooled at four positions by the thermofluid, which is circulated and cooled by an external freeze controller (Tango Nuevo thermostat by Peter Huber Kaeltemaschinenbau GmbH, Offenburg, Germany). Pure ethanol was used as thermofluid. The acrylic glass lid allows

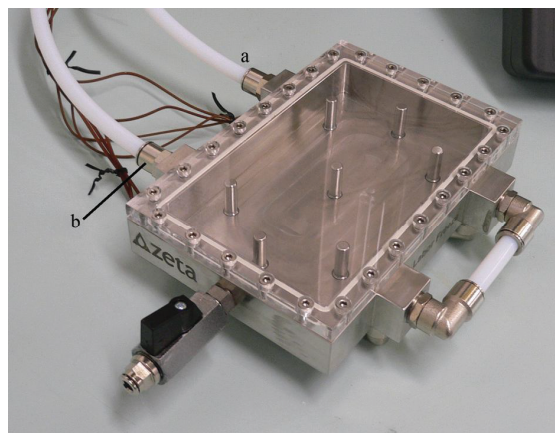


**Figure 1.** The Zeta laboratory-scale freeze container with a total volume of 300 mL consists of a stainless steel jacket with seven bottom-mounted temperature probes, an inlet/outlet valve, and an acrylic glass lid. Ethanol was used as thermofluid and was circulated from the external freeze controller to the upper right connector of the vessel (a), leaving it at the upper left connector (b).

visual observation of the F/T process. Drill core sampling occurred directly from the frozen solution. During the F/T processes, the laboratory-scale freeze container was placed in a polystyrene box for thermal insulation.

Process temperatures were measured with an 8-channel PCE-T 800 Multi-Input thermometer. Sample temperature was  $20 \pm 1^\circ\text{C}$  at the start. The thermofluid was equilibrated for 10 min to  $20^\circ\text{C}$ . Set temperature was then lowered to  $-40^\circ\text{C}$  yielding maximum cooling rate. No seeding was performed to ensure process-near conditions. Sampling occurred exactly 2 h after that. Using a hollow drill with 9-mm inner diameter, frozen core samples of  $0.41 \pm 0.23 \text{ g}$  were taken. To accomplish sampling over the whole depth of the ice block (14 mm in the liquid, slightly thicker in the frozen state), the sampling hole was drilled as deep as possible and remaining material was withdrawn manually using chilled tweezers. Samples were thawed at room temperature and chilled on ice for immediate analysis.

### Concentration and Activity

Bovine serum albumin was used for cryoconcentration studies and LDH was analyzed in terms of F/T stability with respect to sampling position. Protein concentration was measured as described by Bradford<sup>16</sup> employing Roti–Nanoquant assays (Carl Roth) calibrated with BSA. Phosphate was measured as described by Saheki et al.<sup>17</sup> BSA experiments were repeated four times ( $n = 4$ ), and LDH experiments were three times ( $n = 3$ ).

For the determination of specific LDH activity, the conversion of 89 mM L-lactate and 4.5 mM  $\text{NAD}^+$  to pyruvate and NADH (TRIS buffer, 50 mM, pH 8) was followed spectrophotometrically at 340 nm and  $37^\circ\text{C}$  (Beckman Coulter DU 800 spectrophotometer). Contour plots were generated using SigmaPlot 9.0. Statistical significance between cryoconcentration ratios was tested using a Mann–Whitney U-test.

### Thermography

We used a B620 camera by FLIR (Wilsonville, Oregon), mounted in a distance of 50 cm above the laboratory-scale freeze container for thermal imaging of the freezing of 200 mL BSA solution. Emissivity was set to 0.96 for water. For imaging, the acrylic glass lid was removed to allow infrared measurement at the solution surface. Also, insulation was omitted in order to allow for accurate estimation of heat transfer coefficients (HTCs).

### Fluorescence Spectroscopy

A Hitachi F-4500 fluorescence spectrophotometer (Hitachi High-Technologies Corporation, Tokyo, Japan) equipped with a Julabo F25 refrigerated/heating circulator was used to analyze the supernatant of centrifuged samples at  $25(\pm 1)^{\circ}\text{C}$ . Measurements were carried out within 24 h after sampling. Intrinsic protein fluorescence was recorded at 340 nm following excitation at 280 nm. The protein concentration in the sample was  $20\ \mu\text{g}/\text{mL}$ . For measurement of ANS binding to LDH,  $8\ \mu\text{L}$  of a  $50\text{-}\mu\text{M}$  ANS solution (in water) was mixed with  $180\ \mu\text{L}$  of LDH solution ( $20\ \mu\text{g}/\text{mL}$ ) at  $25(\pm 1)^{\circ}\text{C}$ , corresponding to a molar ANS/protein ratio of 4. Exactly 5 min after the mixing, the fluorescence of the solution was measured at 470 nm using excitation at 388 nm. A 5-nm slit width was applied in all fluorescence measurements. Three spectra per sample were recorded, averaged, and smoothed three times with a Savitzky–Golay filter (third order, 50 points). Not F/T-subjected, but otherwise identical samples were used as negative controls.

### Aggregate Detection

A Merck Hitachi LaChrom liquid chromatography system coupled to a model L-7480 fluorescence detector was used for SE-HPLC. The peak area of native LDH tetramer was measured using a TSK-GEL G3000SWXL column that was further equipped with a guard column from Tosoh Bioscience, Tokyo, Japan. A solution of 50 mM potassium phosphate buffer, pH 7.5, with 0.3 M NaCl was used as mobile phase with a flow rate of 0.35 mL/min. Column temperature was held at  $30^{\circ}\text{C}$ . One-hundred microliter of the centrifuged samples was injected after dilution to a protein concentration of  $10\ \mu\text{g}/\text{mL}$ . Fluorescence was measured at 345 nm following excitation at 280 nm. Calibration of the native LDH tetramer peak was performed between 1 and  $50\ \mu\text{g}/\text{mL}$  total protein concentration.

Turbidity was measured spectrophotometrically as absorbance at 400 nm. Calibration with formazin reference solutions was performed according to the European Pharmacopoeia between 3 and 30 nephelometric turbidity units (NTU).<sup>18</sup>

### CFD Modeling

According to Worster and Wettlaufer,<sup>19</sup> there are two possible modes of convection during a solidification process: first, the mushy layer mode driven by the buoyancy in the mushy layer (the porous matrix at the liquid/solid interface) and, second, the boundary layer mode driven by the buoyancy in the region adjacent to the mushy layer in a region called the compositional boundary layer where the freezing process is initiated. The first mode involves the entire mushy layer and is accompanied by a large flux of solute. In contrast, the second mode is small scale and does not penetrate far into the mushy layer. It is accompanied by a very small flux, which is mostly located in the interstices of the mushy layer.

To define a model that can reproduce the above-mentioned modes, the equations of mass conservation, momentum and energy must be solved in a multiphase setup, describing the change of phase (e.g., mass transfer from the liquid phase to the solid phase and vice versa) and the convective effect inside the liquid phase (e.g., convective transport of the solute). One of the challenges is the simultaneous presence of two phases in the same control volume. As the simulated volume can contain volume fractions of both phases at the same time, the solid phase is described as a porous medium. To track the solidification–thawing front effectively on a fixed grid, our method employs a multifluid modeling approach in conjunction with an enthalpy–porosity technique. A two-fluid model involving a liquid and a solid (porous) phase is applied. In contrast to the fluid flow velocities, which can be finite, the velocities in the porous region are associated with zero magnitude.<sup>20</sup> No additional source terms (e.g., Darcy effects) or variable viscosity methods are required to realize zero flow in the solid region.

To accommodate the presence of a solid and a liquid phase, a multifluid method was applied. In this model, each phase is considered as an interpenetrating continuum where the conservation laws are applied. This was necessary to assign different material parameters to a liquid and a solid phase. The continuity equations for each phase (in this case liquid–water and ice–solid) were written in the form indicated by Drew and Passman<sup>21</sup> as follows:

$$\frac{\partial \phi_k \rho_k}{\partial t} + \nabla \cdot \phi_k \rho_k \mathbf{u}_k = \sum_{l=1, l \neq k}^N \Gamma_{kl}, \quad \sum_{k=1}^N \phi_k = 1 \quad (1)$$

where,  $\mathbf{u}_k$  is the velocity vector,  $\phi_k$  is the volume fraction,  $N$  is the total number of phases, and  $\rho_k$  is the density of the phase  $k$ . The right-hand side of Eq. 1 describes the source term related to the phase change that is calculated as:

$$\Gamma_{kl} = \rho_k \cdot \frac{d(\Delta H / h_{fg})}{dt} \quad (2)$$

where  $h_{fg}$  is the latent heat of crystallization and  $\Delta H$  being the latent heat content in the cell.

Momentum and continuity equations according to Drew and Passman<sup>21</sup> are:

$$\frac{\partial \phi_k \rho_k \mathbf{u}_k}{\partial t} + \nabla \cdot \phi_k \rho_k \mathbf{u}_k \mathbf{u}_k = -\phi_k \nabla p + \nabla \cdot \phi_k \rho_k \boldsymbol{\tau}_k + \mathbf{M}_k + \mathbf{u}_k \sum_{l=1, l \neq k}^N \Gamma_{kl} + \mathbf{s}_b \quad (3)$$

where  $p$  is the pressure,  $\mathbf{s}_b$  is the source term of buoyancy, see Eq. 9,  $\boldsymbol{\tau}_k$  is the stress tensor of the phase  $k$ , and  $\mathbf{M}_k$  is the interfacial momentum transfer vector between the phases, with drag being the most important force. The implemented interfacial momentum source, including the drag forces, is given by:

$$\mathbf{M}_c = C_D \frac{1}{8} \rho_c A_{\text{int}} |u_r| u_r = -\mathbf{M}_d \quad (4)$$

The subscript  $k$  is replaced by the subscript  $c$  or  $d$  denoting the continuous (water–protein solution) and dispersed (ice)

phase.  $A_{\text{int}}$  is the interfacial area between the phases that can be calculated from the volume fraction of the disperse phase and a bubble diameter  $D_b$  (which must be defined by the user) as follows:

$$A_{\text{int}} = \frac{6 \varphi_d}{D_b} \quad (5)$$

The relative velocity between continuous and dispersed phase is defined as:

$$u_r = u_d - u_c \quad (6)$$

The drag coefficient is given as:

$$C_D = \begin{cases} \frac{24}{\text{Re}_b} \left(1 + 0.15 \text{Re}_b^{0.687}\right) & \text{Re}_b \leq 1000 \\ 0.438 & \text{Re}_b > 1000 \end{cases} \quad (7)$$

where the Reynolds number  $\text{Re}_b$  is a function of a bubble diameter  $D_b$  and of the liquid phase kinematic viscosity  $\nu_c$ .

$$\text{Re}_b = \frac{u_r D_b'}{\nu_c} \quad (8)$$

In Eq. 3, the buoyancy forces constitute the source term  $S_b$  given by:

$$S_b = \rho_{\text{ref}} g \beta_T (T - T_{\text{ref}}) \quad (9)$$

$\beta_T$  is the linear expansion coefficient implemented in the Boussinesq approximation,<sup>20</sup>  $T$  is the temperature,  $g$  is the gravitational acceleration vector, and  $\rho_{\text{ref}}$  and  $T_{\text{ref}}$  are the reference density and temperature, respectively (293.15 K, 101.325 kPa).

The enthalpy modeling can be realized applying either a homogenous mixture model or a two-fluid static or total enthalpy formulations with detailed interfacial heat transfer exchange between the liquid and solid phases. In this work, the total enthalpy conservation is used and can be expressed as follows:

$$\frac{\partial \varphi_k \rho_k h_k}{\partial t} + \nabla \cdot \varphi_k \rho_k u_k h_k = \nabla \cdot \varphi_k q_k + \rho_m q_k''' + \varphi_k \rho_k g \cdot u_k + \nabla \cdot \varphi_k \tau_k \cdot u_k + \varphi_k \frac{\partial p}{\partial t} + \sum_{l=1, l \neq k, l \in N}^N H_{kl} \quad (10)$$

where  $h_k$  is the enthalpy,  $q_k'''$  is the enthalpy volumetric source,  $q_k$  is the vector of the heat flux,  $H_{kl}$  is the energy interfacial exchange between phases, and  $\rho_m$  is the average density in the cell.

All presented equations were already implemented in the commercial CFD code FIRE<sup>TM</sup> (AVL List GmbH, Graz, Austria) and were solved with this code. In regard to phase change modeling, two input parameters were required, namely, the latent heat (e.g., water 334 kJ/kg) and the freezing point (273.15 K), respectively. In previous investigations,<sup>22</sup> the water freezing process was validated using the numerical and experimental data provided by Giangi et al.,<sup>23</sup> whereby the geometry was a simple cube. Two opposite cube faces were kept at constant temperatures ( $T = 10^\circ\text{C}$  and  $-10^\circ\text{C}$ , respectively), whereas the

lateral walls were set adiabatic. Authors showed that the buoyancy effects are correctly modeled and that they affect the ice-front time evolution as well. A very good agreement with the numerical and experimental data from the literature is shown. All required numerical settings for this work were taken from Iannuccelli et al.<sup>22</sup> As mentioned earlier, the laboratory-scale freeze container consists of a stainless steel box, which is connected to the thermofluid from four sides. Therefore, temperature boundary conditions are very important and special treatment was required. The container jacket was considered in the simulation as well as the transient heat transfer through the metal. Additionally, the heat transfer between the environment and the considered simulation system was included by definition of the “convective heat transfer” (CHT) boundary condition. The required additional input parameters are environment temperature and external HTC. Typical values of HTCs over various shapes for steel and air vary between 2 and 23 W/(m<sup>2</sup> K).<sup>24,25</sup> From our experience with thermal imaging of the nonthermal isolated laboratory-scale freeze container, the best agreement with the experimental data was achieved by the consideration of all above-mentioned domains and accurate thermal boundary conditions.

## RESULTS AND DISCUSSION

### Monitoring of Temperature During Freezing

Thermographical temperature measurements served to initially adjust CFD parameters in an experiment where thermal container insulation of the laboratory-scale freeze container was omitted. Other experiments (with insulation) were used to assess the predictive performance of the model in terms of temperature and cryoconcentration. Seven probes installed inside of the laboratory-scale freeze container recorded the solution temperature throughout the freezing process. Figure 2 shows the progress of the temperatures in 200 mL of a 100- $\mu\text{g/mL}$  LDH solution, the set temperature, and the thermofluid temperature over time. The presence of pure liquid, liquid together with solid as well as completely solidified solution can be distinguished from the diagram: after the initial cooling phase (phase A), the onset of crystallization is indicated by a plateau (phase B) that is recognized in the graphs of the inner probes (positions A, D, and G, Fig. 3). The plateau occurs as a consequence of the heat of crystallization being released during the freezing concomitant with permanent cooling. The probes near the container jacket regions where heat transport to the thermofluid occurs (positions B, C, E, and F, Fig. 3) registered steadily decreasing temperatures straight below  $0^\circ\text{C}$  in the absence of a plateau. The inner probes recorded temperatures of around  $0^\circ\text{C}$  until these positions were incorporated by the ice as well, and the indicated temperature then dropped below  $0^\circ\text{C}$  (phase C). Final temperatures varied between  $-23.0^\circ\text{C}$  and  $-30.1^\circ\text{C}$  depending on the probe positions (Fig. 3). The laboratory-scale freeze container exhibited a relatively small specific heat exchange area (approx. 0.2 cm<sup>2</sup>/mL) and large HTCs [up to 23 W/(m<sup>2</sup> K)] in comparison to small vials [approx. 7 cm<sup>2</sup>/mL, up to 11 W/(m<sup>2</sup> K)]<sup>26</sup> that have also been applied to F/T studies of protein solutions. Moreover, the freeze container provided very rapid cooling of the thermofluid. Therefore, these characteristics of the freeze container setup resulted in the generation of steep temperature gradients at the container walls. Ice nucleation at the walls occurred within minutes under promotion

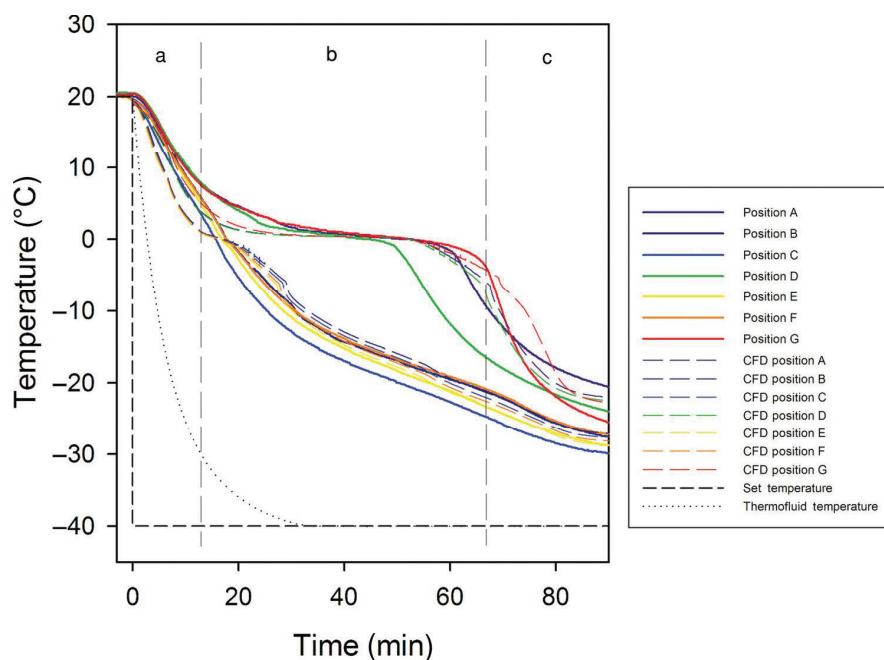


**Figure 2.** Temperature probe measurements of freezing 200 mL LDH solution (100  $\mu\text{g}/\text{mL}$ ) and comparison with corresponding results from CFD simulations. Solid lines represent measured values; dashed lines of the same color represent simulated temperatures in the respective position. (a) Initial cooling phase. (b) Freezing phase. (c) Equilibration to final temperatures. For exact probe location, see Figure 3.

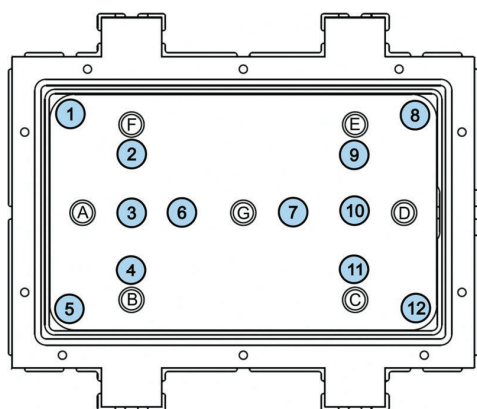


**Figure 3.** Scheme of the arrangement of temperature probes (a–g) and sampling positions (1–12) in the laboratory-scale freeze container.

by natural convection. For that reason, only minimal volumes could have experienced supercooling under these conditions, and this explains why supercooling was not detected in thermal measurements. Note also that the lack of supercooling phenomena was reported in literature using comparable instrumental setups.<sup>13–15</sup>

Additionally, the lack of a plateau formation at the peripheral probes (positions B, C, E, and F, Fig. 3) can be attributed to high-temperature gradients and marginal supercooling in the first minutes of the freezing process. As confirmed by thermographic imaging, freezing temperature was reached at the peripheral probes practically at the same time as they were enclosed by the ice front. The small plateau that was expected

from the simulation at the peripheral probes (Fig. 2) is thus regarded as slight overestimation of phase transition time because of the chosen set of boundary conditions.

Figure 2 shows the corresponding temperatures from the CFD simulation. Generally, there was good agreement of the simulation with the measured temperatures. Only in position D we observed a considerable delay of the simulated ice incorporation of the probe. This is ascribed to the problem of accurate definition of boundary condition of the CFD model under conditions of insufficient thermoinsulation of the laboratory-scale freeze container and the resulting inhomogeneous heat losses. As a consequence, the effect of more efficient heat exchange and thereby lower temperatures on the right side of the container (see Fig. 1: thermofluid inflow at A) seems to be underestimated in the model. An improvement of thermal isolation will however allow for more precise definition of simulation boundary conditions and should lead to an increased precision of the predictions.

Visualization of the freezing process with simultaneous temperature measurement at the solution surface was accomplished with infrared thermography. The comparison with temperatures from CFD simulations served to optimize the performance of the CFD model in terms of definition of appropriate boundary conditions. Figure 4 pictures the agreement of simulation (after model optimization) and experiment in the case of a BSA solution frozen down to as low as  $-34^{\circ}\text{C}$ , measured thermographically. The delay of the time point of complete solidification compared with the probe measurements (Fig. 2) can be explained by the omission of the acrylic glass lid and the polystyrene box and the associated loss of thermal isolation. Phase transition in the simulation lasted 4 min longer than measured. Nevertheless, with temperature probe

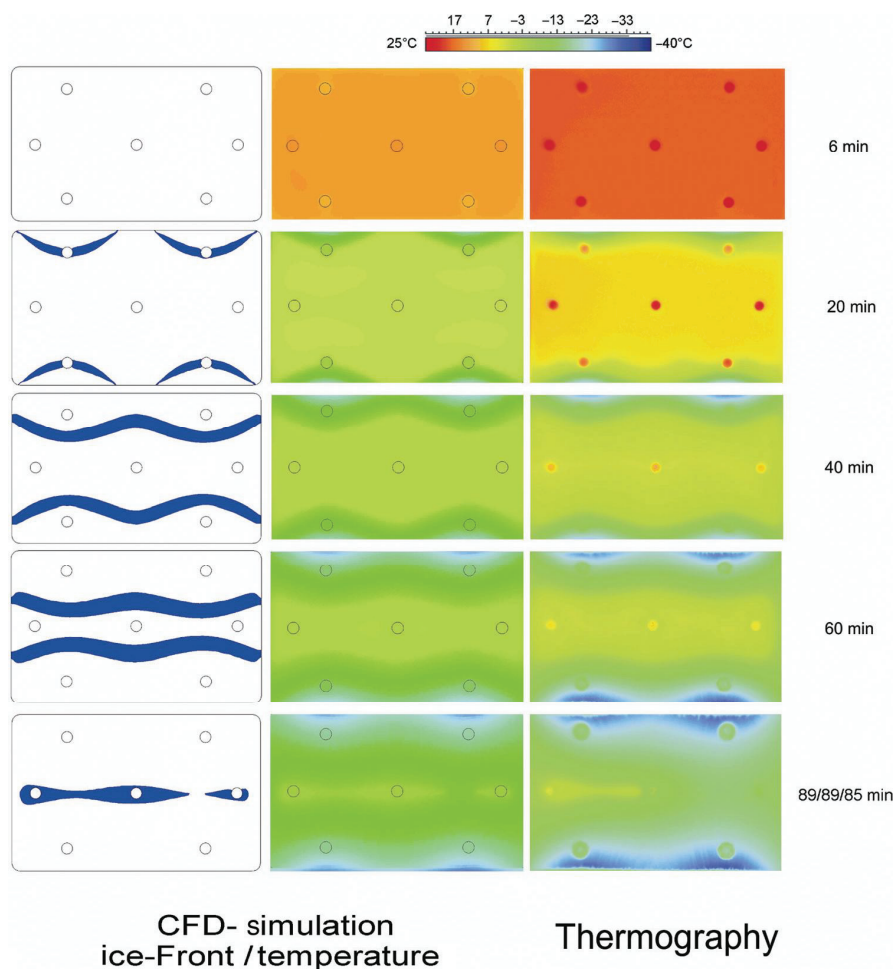


**Figure 4.** Alignment of CFD temperature simulations with thermographic measurement during freezing 200mL BSA solution. Infrared thermography served to initially adjust CFD parameters. The propagation of the ice front (left, blue) can be followed to the last freezing spot in minute 89 (CFD) and 85min (thermography), respectively.

measurements, we can affirm that the used CFD model is capable of predicting the temperature dynamics and the phase separation in the presented laboratory-scale freeze container.

Particularly, the identification of the last freezing spots is of crucial interest for the design of a freeze container. Unlike with the used laboratory-scale freeze container, visual inspection is usually impossible for an industrial scale device. Reliable process surveillance depends on temperature measurements and the optimal placement of temperature probes in those regions.<sup>27</sup> In the current case, we observed an asymmetric solidification behavior. The position where the solution remained liquid for the longest time was found between temperature probes A and G on the thermofluid outflow side of the container (see Figs. 3 and 4). This was because of the higher heat transport from the other side of the container, the inflow side, where the circulating thermofluid had a lower temperature.

Using thermography together with visual inspection, we obtained evidence suggesting that the used stainless steel thermal probes did not affect crystallization. The area immediately surrounding the probes at about 4 mm distance exhibited iden-

tical freezing behavior as the relevant area more distant (33–45 mm) from the probe. The probes did not induce crystallization, but they also did not seem to hinder it. Temporary, solution temperatures directly at the probe surfaces slightly exceeded bulk temperatures (usually  $<1^{\circ}\text{C}$ , maximum  $2.3^{\circ}\text{C}$ ). However, as this occurred only within a distance of less than 1.8 mm from the probe surface, we consider interference with our concentration measurements to be negligible. Also, the slight temporary overestimation of bulk temperature as a consequence of the probe contribution does not interfere with the overall outcome of the present study. In summary, therefore, probes used for local temperature determination are believed to be largely noninvasive in respect to influencing the system's freezing behavior.

The used CFD model thus serves to predict the last freezing spots for this flat, approximate two-dimensional freezing system with adequate accuracy. The applicability of the model to a three-dimensional container geometry yet needs to be demonstrated. However, even with this system, we found that solidification was delayed longest at the air–liquid surface of the last freezing spots, which was also seen in the CFD simulation.

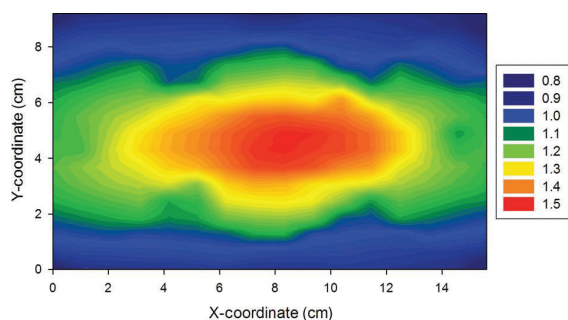


**Figure 5.** Contour plot comprising 24 concentration measurements throughout the laboratory-scale freeze container after freezing 200 mL BSA solution. Plotted was the relative concentration compared with the initial value. ( $n = 4$ , mean).

### Cryoconcentration of Solutes

Spontaneous water crystallization upon cooling of the protein solutions below  $0^{\circ}\text{C}$  led to a continuous increment of solute concentrations in the remaining liquid phase because of the rejection of solutes from the ice phase. The spatial characteristics of macroscopic cryoconcentration were equivalent for BSA, LDH, and phosphate. Figure 5 shows an interpolated contour plot representing the BSA concentration determined in 24 positions in the frozen solution. Highest concentrations of BSA were found in the central region of the laboratory-scale freeze container, around the longitudinal axis. Here, we found protein concentrations of up to 153% of the initial value. In side regions that used to freeze first the concentrations dropped as low as 82% yielding a cryoconcentration ratio of  $2.00 \pm 0.30$  (highest concentration/lowest concentration).

Samples from LDH stability experiments were withdrawn in the positions 1–12 as shown in Figure 3. Concentrations of LDH and phosphate are shown in Figure 6. Cryoconcentration ratios were  $3.11 \pm 0.61$  for LDH and  $3.40 \pm 0.70$  for phosphate. Looking at each sampling position, we found qualitative agreement of cryoconcentration patterns of LDH and phosphate with BSA. Local concentration minima were identified at positions 2, 4, 9, and 11. The region of the highest solute concentration was found in the symmetric middle—the longitudinal axis of the container. This was also the region that could be clearly identified as the last point of freeze (Fig. 4). This indicates that

the used CFD model can be used to localize regions of highest macroscopic cryoconcentration by identifying the last freezing spots in the container. There is a slight discrepancy between the actual last freezing spot lying in the left side (thermofluid outflow) of the container and the point with the highest macroscopic concentration in the very symmetric middle. This can be explained by the contribution of larger volumes to cryoconcentration in the middle regions compared with the side regions, together with the temperature gradient originating from the asymmetric circulation of thermofluid from the inflow to the outflow side of the container, leading to a delay of phase transition.

However, knowledge about the distribution pattern of the protein within the laboratory-scale freeze container is essential for process understanding and is directly related to the question where to place analytical probes or devices for temperature control or mixing. We were able to accurately simulate temperature and phase transition during the process of freezing protein solutions in the laboratory-scale freeze container and thereby identify regions with high solute cryoconcentration.

Despite the large differences in molecular mass, phosphate cryoconcentration consistently resembles LDH concentrations. Eutectic concentrations (2.7 M for  $\text{K}_2\text{HPO}_4$  and 1.3 M for  $\text{KH}_2\text{PO}_4$ <sup>28</sup>) were not reached in phosphate measurements, extensive precipitation of phosphate salts is therefore improbable.

However, an excess of the limits in the microscopic scale cannot be precluded and might remain a risk for enzyme inactivation.

The extent of cryoconcentration of BSA was found to be significantly lower than cryoconcentration of both LDH and phosphate (cryoconcentration ratios were  $3.11 \pm 0.61$  for LDH,  $3.40 \pm 0.70$  for phosphate and  $2.00 \pm 0.30$  for BSA,  $p < 0.05$ ). The reason for this is not clear. The moderate increase in solidification time during freezing of BSA because of the worse-insulated container would rather have increased cryoconcentration ratios for BSA as compared with LDH or phosphate. Adsorption of BSA to the negatively charged ice surface<sup>29</sup> seems very unlikely because of its own negative charge at pH 7.5 and the positive charge of the LDH tetramer.<sup>30</sup> A slight drop of pH (0.2–0.3 units) might have occurred during freezing.<sup>31,32</sup> However, this shift could not have altered electrostatic conditions in a way favoring BSA adsorption.<sup>29,30</sup>

Also, higher solubility of BSA at temperatures close to or below  $T_m$  could explain different cryoconcentration levels of

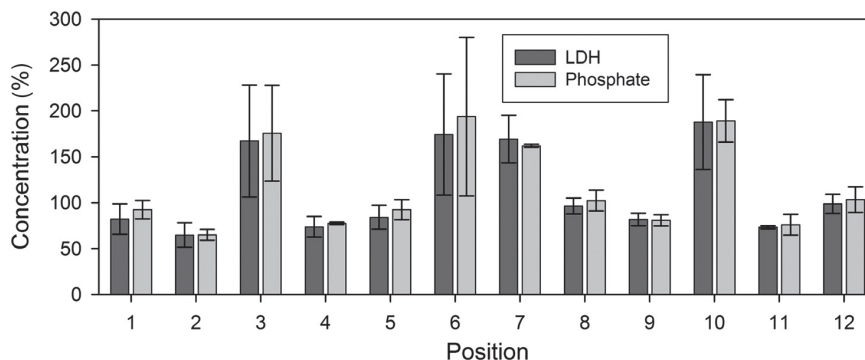


**Figure 6.** Concentration of LDH and phosphate after freezing in positions 1–12 (see Fig. 3), relative to initial concentrations. ( $n = 3$ , mean  $\pm$  SD).

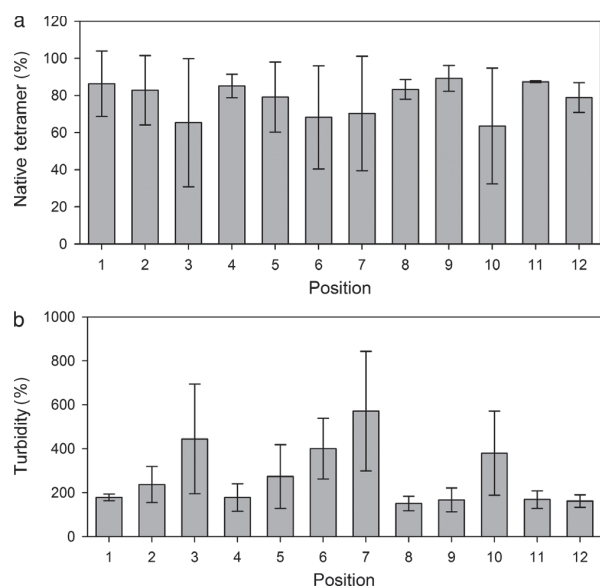


**Figure 7.** (a) Amount of native LDH tetramer identified with SE-HPLC in positions 1–12 relative to unfrozen control. ( $n = 3$ , mean $\pm$ SD). (b) Turbidity in positions 1–12 relative to unfrozen control ( $4.5\pm 1.3$ NTU). ( $n = 3$ , mean $\pm$ SD).

the two proteins. Higher equilibrium concentrations of BSA near the water–ice interface, and therefore higher probability for BSA to be enclosed by the growing ice front, would result in reduced BSA–cryoconcentration. However, temperature-dependent solubility data for BSA and LDH supporting this notion were not found and investigations addressing this question were out of the scope of this work.

Also, structural perturbations could explain the large deviations of cryoconcentration levels. Although no irreversible unfolding of LDH because of F/T was detected in this study, cold denaturation has been observed for LDH in earlier work.<sup>33,34</sup> Extensive unfolding however would rather result in reduced cryoconcentration of LDH because of the loosening of the native structure and an increased probability to adsorb to the ice surface.<sup>1,35</sup> Also, no significant loss of quaternary structure of LDH was detected using SE-HPLC. BSA, on the contrary, proved excellent stability toward F/T stresses in many cases. Nevertheless, (partial) unfolding of BSA during freezing and/or BSA adsorption to the ice surface seem to be the most plausible explanations for the significantly lower cryoconcentration levels of BSA compared with LDH.

#### Stability of LDH in a Laboratory-Scale Freeze Container

L-Lactic dehydrogenase is known to be sensitive to F/T stresses. At concentrations around and below 100  $\mu\text{g}/\text{mL}$  unfolding, aggregation and inactivation can occur after a single F/T cycle.<sup>7,9,36</sup> Principal cause of F/T-related LDH inactivation appears to be the contact with the ice surface.<sup>37</sup> The notion is supported by the finding that LDH is stabilized against F/T by preferentially excluded cosolutes.<sup>38</sup>

We assessed the overall freeze damage by measuring the specific activity of LDH catalyzing the oxidation of lactate to pyruvate. Core samples 1–12 from the frozen solution did not exhibit significant changes in activity compared with controls

that were measured without freezing or were kept at 4°C. A slight trend for higher activity retention was found in concentrated regions. Higher LDH concentrations are known to be less susceptible to F/T stresses at small milliliter scale<sup>9</sup> as commonly observed for proteins.

Structural perturbation was probed using intrinsic tryptophane fluorescence and ANS fluorescence. No evidence for protein unfolding could be observed for samples from cores 1 to 12. For the detection of protein aggregates, we applied turbidimetric measurements for the fraction of visible particles and SE-HPLC for multi- and oligomeric aggregates. The latter method did not provide evidence for the presence of LDH aggregates. However, the inner sampling positions 3, 6, 7, and 10 exhibited the lowest amounts of native tetramer while showing the highest turbidity values (Fig. 7).

Rabbit muscle LDH was unexpectedly resistant against F/T stresses in the used laboratory-scale freeze container. Earlier studies as well as our own observations in small milliliter volumes showed that LDH is susceptible to inactivation and structural perturbation upon (repeated) F/T.<sup>7,9,36</sup> Despite substantial cryoconcentration of protein and phosphate, we did not detect any loss of activity or native conformation. It appears that in the current case cryoconcentration of LDH in the absence of extensive precipitation of buffer salts or other excipients had a cryoprotective effect on protein stability against destabilizing factors such as ice surface exposure or minor buffer-specific pH shifts,<sup>31,32</sup> as suggested before.<sup>39</sup> Aggregation was low and could only be detected as increased turbidity in the highly concentrated regions of the container. However, also the insignificant loss of native LDH tetramer as detected with SE-HPLC in the same regions suggests LDH aggregation. The notion of stabilization by protein cryoconcentration is not contradicted by the finding of aggregates in the concentrated regions given that aggregates encounter the same cryoconcentration effects as other solutes. Potential reversibility of aggregation and/or unfolding cannot be ruled out, though we strove for minimizing the gaps between thawing and analysis. Lowering the initial LDH concentration would certainly increase the chance of destabilization, aggregation, and activity loss. At the same time, however, the chance for the detection of these effects would suffer as we are already moving near the detection limits of the employed methods with the concentration used in this study.

#### CONCLUSIONS

We present the analysis of a freezing process in a newly designed and constructed laboratory-scale freeze container. We were able to show that it enables the characterization of a freezing procedure as well as process surveillance and control. As shown for LDH, multiple parameters for protein stability can be acquired for a unit operation with industrial characteristics. The good F/T stability of LDH as well as diverging cryoconcentration levels for LDH and BSA in the laboratory-scale freeze container furthermore underline the necessity of specialized investigations at intermediate volumes, which are possible with the introduced system at a minimum of costs for biopharmaceutical material. The laboratory-scale freeze container qualifies as a pilot device to study protein stability at scale, for process design or as a tool to aid product or formulation development in terms of bulk protein F/T. The identification and analysis of critical process parameters in accordance with QbD principles

is an issue that is of special interest in terms of freezing biopharmaceuticals and is currently under investigation using the Zeta Biopharma laboratory-scale freeze container.

Heat and mass transport as well as phase transition were successfully modeled using CFD. Qualitative and quantitative agreement with experimental results was shown in seven positions after highly resolved calibration of simulation parameters using infrared thermography. The used model helps to predict temperature development as well as the spatial geometry of macroscopic cryoconcentration during a freezing process. It delivers valuable information for future development and scaling of more complex freeze containers such as localization of hot/cold spots, points of highest concentrations, or the transient behavior of the ice interface.

Upcoming generations of the laboratory-scale freeze container will allow the installation of advanced process analytical tools based on the presented simulation techniques. Moreover, optimized thermoisolation will lead to more precise definition of CFD model boundary conditions and thereby more reliable simulation results.

## ACKNOWLEDGMENTS

For financial and technical support and an excellent collaboration, the authors thank Zeta Biopharma, especially Birgit Pittermann, Andreas Gloessel, and Alexander Trausznig. Jakob Woisetschlaeger (Institute for Thermal Turbomachinery and Machine Dynamics, Graz University of Technology, Austria) is thanked for enabling thermographic measurements. We also thank Georg Scharrer from Research Center Pharmaceutical Engineering for his assistance.

This work has been funded within the Austrian COMET Program under the auspices of the Austrian Federal Ministry of Transport, Innovation and Technology (bmvit), the Austrian Federal Ministry of Economy, Family and Youth (bmwfj), and by the State of Styria (Styrian Funding Agency SFG). COMET is managed by the Austrian Research Promotion Agency FFG.

## NOMENCLATURE

$A_{\text{int}}$	interfacial area between the phases ( $\text{m}^2$ )
$C_D$	drag coefficient (dimensionless)
$D_b$	bubble diameter (m)
$g$	gravitational acceleration ( $\text{m/s}^2$ )
$h_{\text{fg}}$	latent heat of crystallization ( $\text{J/kg}$ )
$\Delta H$	latent heat content in the cell ( $\text{J/kg}$ )
$H_{\text{kl}}$	energy interfacial exchange between the phases (W)
$M_c$	interfacial momentum transfer vector in the continuous phase (N)
$M_d$	interfacial momentum transfer vector in the dispersed phase (N)
$M_k$	interfacial momentum transfer vector between the phases (N)
$N$	number of phases (dimensionless)
$p$	hydrodynamic pressure (Pa)
$q'''$	enthalpy volumetric source (W/kg)
$q_k$	vector of the heat flux (W)
$R_a$	surface roughness ( $\mu\text{m}$ )
$Re_b$	Reynoldsnumber (dimensionless)
$S_b$	source term of buoyancy (dimensionless)
$t$	time (s)

$T$	temperature (K)
$T_g$	glass transition temperature (K)
$T_m$	melting temperature (K)
$T_{\text{ref}}$	reference ambient temperature (K)
$u_k$	velocity vector (m/s)
$u_r$	relative velocity between the phases (m/s)

## Greek Symbols

$\beta_T$	linear expansion coefficient (dimensionless)
$\Gamma_{\text{kl}}$	mass source term (kg/s)
$\nu_c$	kinematic viscosity ( $\text{m}^2/\text{s}$ )
$\rho_k$	density of the phase k ( $\text{kg/m}^3$ )
$\rho_m$	average density in the cell ( $\text{kg/m}^3$ )
$\rho_{\text{ref}}$	reference ambient density ( $\text{kg/m}^3$ )
$\tau_k$	stress tensor of the phase k (Pa)
$\phi_k$	volume fraction (dimensionless)

## REFERENCES

- Singh S, Kolhe P, Wang W, Nema S. 2009. Large-scale freezing of biologics: A practitioner's review. Part one: Fundamental aspects. *Bioproc Int* 7:32–44.
- Kreilgaard L, Jones LS, Randolph TW, Frokjaer S, Flink JM, Manning MC, Carpenter JF. 1998. Effect of Tween 20 on freeze-thawing and agitation-induced aggregation of recombinant human factor XIII. *J Pharm Sci* 87:1597–1603.
- Kueltzo L, Wang W. 2008. Effects of solution conditions, processing parameters, and container materials on aggregation of a monoclonal antibody during freeze-thawing. *J Pharm Sci* 97:1801–1812.
- Kolhe P, Badkar A. 2011. Protein and solute distribution in drug substance containers during frozen storage and post-thawing: A tool to understand and define freezing-thawing parameters in biotechnology process development. *Biotechnol Prog* 27:494–504.
- Singh SK, Kolhe P, Wang W, Nema S. 2009. Large-scale freezing of biologics: A practitioner's review. Part two: Practical advice. *Bioproc Int* 7:34–42.
- Singh SK, Nema S. 2010. Freezing and thawing of protein solutions. In *Formulation and process development strategies for manufacturing biopharmaceuticals*; Jameel F, Hershenson S, Eds. Hoboken, New Jersey: John Wiley & Sons, pp 625–675.
- Jiang S, Nail SL. 1998. Effect of process conditions on recovery of protein activity after freezing and freeze-drying. *Eur J Pharm Biopharm* 45:249–257.
- Pikal-Cleland K. 2000. Protein denaturation during freezing and thawing in phosphate buffer systems: Monomeric and tetrameric  $\beta$ -galactosidase. *Arch Biochem Biophys* 384:398–406.
- Cao E, Chen Y, Cui Z, Foster PR. 2003. Effect of freezing and thawing rates on denaturation of proteins in aqueous solutions. *Biotechnol Bioeng* 82:684–690.
- Kolhe P, Holding E, Lary A, Chico S, Singh SK. 2010. Large-scale freezing of biologics: Understanding protein and solute concentration changes in a cryovessel-part 1. *Bio Pharm Int* 23:53–60.
- Kolhe P, Holding E, Lary A, Chico S, Singh SK. 2010. Large-scale freezing of biologics: Understanding protein and solute concentration changes in a cryovessel-part 2. *Bio Pharm Int* 23.
- Singh SK, Kolhe P, Mehta AP, Chico SC, Lary AL, Huang M. 2011. Frozen state storage instability of a monoclonal antibody: Aggregation as a consequence of trehalose crystallization and protein unfolding. *Pharm Res* 28:873–885.
- Shamlou PA, Breen LH, Bell WV, Pollo M, Thomas BA. 2007. A new scalable freeze-thaw technology for bulk protein solutions. *Biotechnol Appl Biochem* 46:13–26.
- Radmanovic N, Serno T. 2013. Understanding the freezing of biopharmaceuticals: First principle modeling of the process and evaluation of its effect on product quality. *J Pharm Sci* 102:2495–2507.

15. Rodrigues MA, Balzan G, Rosa M, Gomes D, de Azevedo EG, Singh SK, Matos HA, Geraldes V. 2013. The importance of heat flow direction for reproducible and homogeneous freezing of bulk protein solutions. *Biotechnol Prog* 29:1212–1221.
16. Bradford MM. 1976. A rapid and sensitive method for the quantitation of microgram quantities of protein utilizing the principle of protein-dye binding. *Anal Biochem* 72:248–254.
17. Saheki S, Takeda A, Shimazu T. 1985. Assay of inorganic phosphate in the mild pH range, suitable for measurement of glycogen phosphorylase activity. *Anal Biochem* 148:277–281.
18. Clarity and degree of opalescence of liquids. 2008. *Pharmacopoea Europaea*. 6th edition. Strasbourg, France: : European Directorate for the Quality of Medicine.
19. Worster M, Wettlaufer J. 1997. Natural convection, solute trapping, and channel formation during solidification of saltwater. *J Phys Chem B* 5647:6132–6136.
20. FIRE™ user manual. 2011. Graz, Austria: AVL List GmbH.
21. Drew DA, Passman SL. 1998. *Theory of multicomponent fluids*. New York: Springer.
22. Iannuccelli M, Suzzi D, Sirnik B, Rinderhofer A, Khinast JG. 2011. Numerical simulation of freeze-thaw biopharmaceutical processes. *Chem Eng Trans* 24:907–912.
23. Giangi M, Stella F, Kowalewski TA. 1999. Phase change problems with free convection: Fixed grid numerical simulation. *Comput Vis Sci* 2:123–130.
24. Lienhard J IV, Lienhard JV. *A heat transfer textbook*. Phlogiston Press.
25. Verein Deutscher Ingenieure. 2013. *VDI-Waermeatlas*. Wiesbaden, Germany: Springer Vieweg.
26. Nakagawa K, Hottot A, Vessot S, Andrieu J. 2007. Modeling of freezing step during freeze-drying of drugs in vials. *AIChE J* 53:1362–1372.
27. Hartmann U, Nunner B, Körber C, Rau G. 1991. Where should the cooling rate be determined in an extended freezing sample? *Cryobiology* 28:115–130.
28. Van Den Berg L, Dyson R. 1959. Effect of freezing on the pH and composition of sodium and potassium phosphate solutions: The reciprocal system  $\text{KH}_2\text{PO}_4\text{-Na}_2\text{HPO}_4\text{-H}_2\text{O}$ . *Arch Biochem Biophys* 81:319–329.
29. Čop A, Kallay N. 2004. Surface potential of ice in aqueous electrolyte solutions. *Prog Colloid Polym Sci* 126:83–85.
30. Olsson MH, Søndergaard CR, Rostkowski M, Jensen JH. 2011. Propka3: Consistent treatment of internal and surface residues in empirical  $\text{pK}_a$  predictions. *J Chem Theory Comput* 7:525–537.
31. Williams-Smith DL, Bray RC, Barber MJ, Tsopanakis AD, Vincent SP. 1977. Changes in apparent pH on freezing aqueous buffer solutions and their relevance to biochemical electron-paramagnetic-resonance spectroscopy. *Biochem J* 167:593–600.
32. Pikal-Cleland KA, Cleland JL, Anchordoquy TJ, Carpenter JF. 2002. Effect of glycine on pH changes and protein stability during freeze-thawing in phosphate buffer systems. *J Pharm Sci* 91:1969–1979.
33. Hatley RH, Franks F. 1989. The cold-induced denaturation of lactate dehydrogenase at sub-zero temperatures in the absence of perturbants. *FEBS Lett* 257:171–173.
34. Hatley RH, Franks F. 1989. The effect of aqueous methanol cryosolvents on the heat- and cold-induced denaturation of lactate dehydrogenase. *Eur J Biochem* 184:237–240.
35. Strambini GB, Gonnelli M. 2007. Protein stability in ice. *Biophys J* 92:2131–2138.
36. Zhang A, Qi W, Singh S, Fernandez E. 2011. A new approach to explore the impact of freeze-thaw cycling on protein structure: Hydrogen/deuterium exchange mass spectrometry (HX-MS). *Pharm Res* 28:1–15.
37. Bhatnagar B, Pikal M, Bogner RH. 2008. Study of the individual contributions of ice formation and freeze concentration on isothermal stability of lactate dehydrogenase during freezing. *J Pharm Sci* 97:798–814.
38. Carpenter JF, Crowe JH. 1988. The mechanism of cryoprotection of proteins by solutes. *Cryobiology* 25:244–255.
39. Wang W. 1999. Instability, stabilization, and formulation of liquid protein pharmaceuticals. *Int J Pharm* 185:129–188.

### 3 Visualizing Cryoconcentration of Proteins in a Laboratory-Scale Freeze Container

Ulrich Roessl,<sup>1,2</sup> Stefan Leitgeb,<sup>1</sup> Bernd Nidetzky<sup>1,2</sup>

*1 Research Center Pharmaceutical Engineering GmbH, Graz, Austria*

*2 Institute for Biotechnology and Biochemical Engineering, Graz University of Technology, Austria*

#### **Abstract**

A simple method for the visualization of protein concentration gradients in frozen bulk solutions was developed. Bovine serum albumin (BSA) was conjugated with fluorescein isothiocyanate (FITC) and subjected to different freezing protocols in a laboratory-scale stainless steel container. It could be demonstrated that the rate of heat removal and the time of nucleation influence microscopic cryoconcentration. Size and number of cryoconcentrated regions in the frozen bulk solution varied with the processing parameters. The presented method explicitly illustrates the magnitude of cryoconcentration and aids in appreciation of its consequences.

#### **Abbreviations:**

BSA: Bovine serum albumin, CLSM: Confocal laser scanning microscopy, FITC: Fluorescein isothioyanate, F/T: Freezing and thawing,  $T_m$ : Melting temperature,  $T_g'$  Glass transition temperature of the maximal freeze concentrated matrix

## **Introduction**

Cryoconcentration is a phenomenon that inevitably occurs when an aqueous solution is frozen. Upon lowering the temperature, the probability for ordered water structures to form increases. Below  $T_m$  these clusters can grow as the bulk free energy inside the clusters gets smaller than outside. Growth is opposed by the energy necessary for cluster surface creation, but once a critical size is reached, total free energy drops and nuclei are formed.<sup>1</sup> This nucleation process states the beginning of freezing and involves only water molecules. Solutes or impurities can stabilize water nuclei and thereby facilitate nucleation (heterogeneous nucleation) but are excluded from water crystallization. Thus, solutes are repelled from the growing ice surface. They are either concentrated in warmer regions of the bulk solution or get trapped in between growing ice structures, often exhibiting dendritic growth patterns.<sup>2</sup> The ongoing entrapment of solutes in between water ice crystals causes local compartmentation, often referred to as microscopic cryoconcentration.<sup>3</sup> The accumulation of solutes in the bulk regions which freeze later is called macroscopic cryoconcentration. There, easy measurable concentration gradients are formed between central and peripheral regions of cryovessels.<sup>4</sup> When temperature decreases further, solutes trapped in central or peripheral regions are concentrated in a maximal freeze concentrated matrix at the glass transition temperature ( $T'_g$ ). Storage of pharmaceutical proteins in the frozen state is usually preferred below  $T'_g$  as diffusion is arrested and aggregation is hindered during the storage period.<sup>5</sup>

Since proteins as well as co-solutes undergo cryoconcentration, precipitation or crystallization of buffer components or excipients can occur and thereby impair protein stability.<sup>1,6,7</sup> Thus, the minimization of cryoconcentration effects could be advantageous under certain conditions.

The extent of cryoconcentration can be influenced by the number of ice nuclei that form when freezing starts. When supercooling of the solution can be accomplished the number of nuclei is increased as the critical cluster size is smaller at lower temperatures. When protracting heterogeneous nucleation by using low-particle solutions, high degrees of supercooling can be accomplished applying high cooling rates.<sup>1</sup> For volumes of a few  $\mu\text{L}$  up to 1 mL, cooling rates of 100 K/min and higher can be reached with different techniques.<sup>8</sup> In freezing vessels with higher volumes, comparable cooling rates are not possible. There, fast heat removal generates steep temperature gradients at the walls of the vessel, causing very fast local nucleation instead of a delay in the whole bulk. Thus, in larger volumes slower cooling rates are necessary to reach highest degrees of supercooling, which can range from 5 to 15 °C below  $T_m$ . Very small cooling rates were needed to achieve substantial supercooling in industrial scale freeze containers. Then, however, a high number of smaller cryoconcentrated regions should be formed between water ice crystals. On

the other hand, slow freezing in multi-mL vessels and larger generally causes higher macroscopic cryoconcentration, which can be related to diffusive and convective effects.<sup>4,6,7</sup> This renders process-related control of cryoconcentration levels in bulk-freezing operations very difficult.

In this work we want to describe how patterns of microscopic cryoconcentration in a 200 mL freeze container are influenced by supercooling and the rate of heat removal. We use fluorescently labeled bovine serum albumin (BSA) to visualize effects of cryoconcentration in ice core samples. Different cooling rates allow the evaluation of different phase transition rates as well as the impact of supercooling. Images obtained with confocal laser scanning microscopy (CLSM) will give an impression of the magnitude of concentration gradients caused by freezing and will help raising awareness of the harsh contrast between storage conditions for proteins in the frozen and the liquid state.

## **Materials and methods**

### Materials

BSA was purchased from Sigma-Aldrich, St. Louis, MO, USA. Fluorescein isothiocyanate (FITC) as well as other chemicals and reagents used were from Carl Roth GmbH + Co. KG, Karlsruhe, Germany. Vivaspin ultrafiltration columns from GE Healthcare, Little Chalfont, UK (MWCO 10 kDa), were used for separation of BSA from unbound FITC.

### FITC-labeling of BSA

A standard FITC labeling procedure for proteins was used.<sup>9,10</sup> BSA was dissolved in 0.5 M sodium carbonate buffer, pH 9.5, to yield a concentration of 5 mg/mL. 2.5 mL of FITC in anhydrous dimethyl sulfoxide (DMSO), 1 mg/mL, was added to 20 mL of BSA solution, in 20  $\mu$ l-aliquots under gentle stirring. The preparation was incubated in dark for 12 hours at 4°C. 2.2 mL of a 0.5 M NH<sub>4</sub>Cl solution was then added followed by 2 hours dark incubation at 4°C. Unbound FITC was removed using ultrafiltration columns while buffer was exchanged to 50 mM potassium phosphate buffer, pH 7.5. The ratio of bound FITC molecules per protein molecule (F/P) was determined using the following equation:

$$\text{Molar } F/P = \frac{MW}{389} \times \frac{A_{495}/195}{A_{280} - [(0.35 \times A_{495})]/E_{280}^{0.1\%}}$$

where  $MW$  = molecular weight of BSA (66,433 Da), 389 is the molecular weight of FITC, 195 = absorption  $E^{0.1\%}$  of bound FITC at 490 nm and pH 13.0,  $(0.35 \times A_{495})$  = correction factor due to the absorbance of FITC at 280 nm,<sup>11</sup>  $E_{280}^{0.1\%}$  = absorption of BSA at 280 nm at 1.0 mg/ml (0.614).  $A_{280}$  and  $A_{495}$  = absorbances measured at the respective wavelengths on a Beckman Coulter DU 800 spectrophotometer. Also, BSA concentration was determined spectrophotometrically using the absorbance at 280 nm.

## Freezing and sampling

200 mL of labeled BSA solution, 0.1 mg/mL, were subjected to freezing in a 200 mL laboratory freeze-container manufactured by Zeta Biopharma GmbH, Lieboch, Austria, which was described in detail elsewhere.<sup>12</sup> Silicone oil (M40.165.10 by Peter Huber Kaeltemaschinenbau GmbH, Offenburg, Germany) was used as thermofluid. For freezing the thermofluid was cooled to a set temperature of  $-40^{\circ}\text{C}$  using four different protocols. Process temperatures were measured with an 8-channel PCE-T 800 Multi-Input Thermometer. Measurements occurred at seven positions, indicated as A-G in Figure 1. Phase transition time was measured as the time between nucleation and complete solidification of the bulk, which can be identified as a plateau in temperature profiles. When seeding was performed, frozen buffer droplets were introduced next to the cooled container walls as soon as a bulk temperature of  $-2^{\circ}\text{C}$  was perceived. After freezing and equilibration of bulk temperatures, the ice block was removed from the container. Samples were drilled from the frozen ice block using a hollow drill with an inner diameter of 25 mm. Three samples were taken from each run from positions 1-3 as indicated in Figure 1. Ice cores were stored in 50 mL Falcon tubes at  $-70^{\circ}\text{C}$  until microscopic examination.

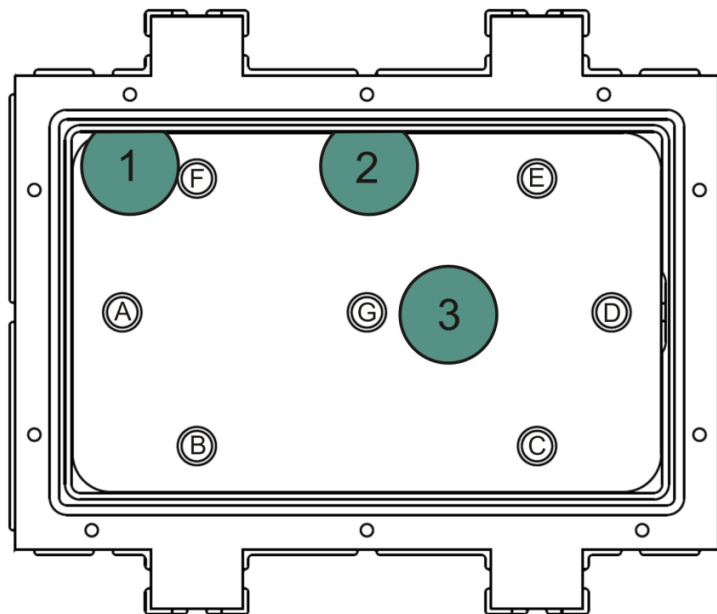


**Figure 1: Schematic illustration of the freeze container indicating sampling positions 1-3. CLSM images were taken from central regions of the ice core samples. At positions A-G thermocouples were placed for temperature monitoring.**

### Confocal laser scanning microscopy (CLSM)

CLSM images from frozen samples were taken with a Leica DMI 6000 inverted microscope in a TCS SP5 system, Leica Microsystems GmbH, Wetzlar, Germany. Excitation occurred at 488 nm, acquisition from 502 - 603 nm. Magnification was 630fold. For the measurements samples were placed in a plastic dish with a glass slide bottom while dry ice was used for cooling.

## Results

A molar F/P ratio of 3.4 was reached after FITC-labeling of BSA. Four different freezing protocols were applied to obtain different phase transition times. Immediate lowering of the set temperature to  $-40^{\circ}\text{C}$  led to a phase transition time of 53 min. Here, no seeding was necessary as the rapid lowering of temperature led to immediate nucleation at the container walls. In a second experiment, the set temperature was lowered to  $-40^{\circ}\text{C}$  linearly over 4 h. Seeding was performed and the phase transition took 87 min. Decreasing temperature to  $-40^{\circ}\text{C}$  within 12 h led to a phase transition lasting 4 h 22 min after seeding. Linear temperature decrease in 4 h without seeding resulted in a phase transition time of only 73 min. Supercooling was achieved for the whole bulk yielding  $-4.6^{\circ}\text{C}$  in peripheral and  $-1.0^{\circ}\text{C}$  in central regions right before spontaneous nucleation. Ice core samples were examined using CLSM, and images were collected as fast as possible before any sample melting through laser beam exposure would occur. Representative images for every position of the four experiments are shown in Figure 2. Images were arranged by position and phase transition time.

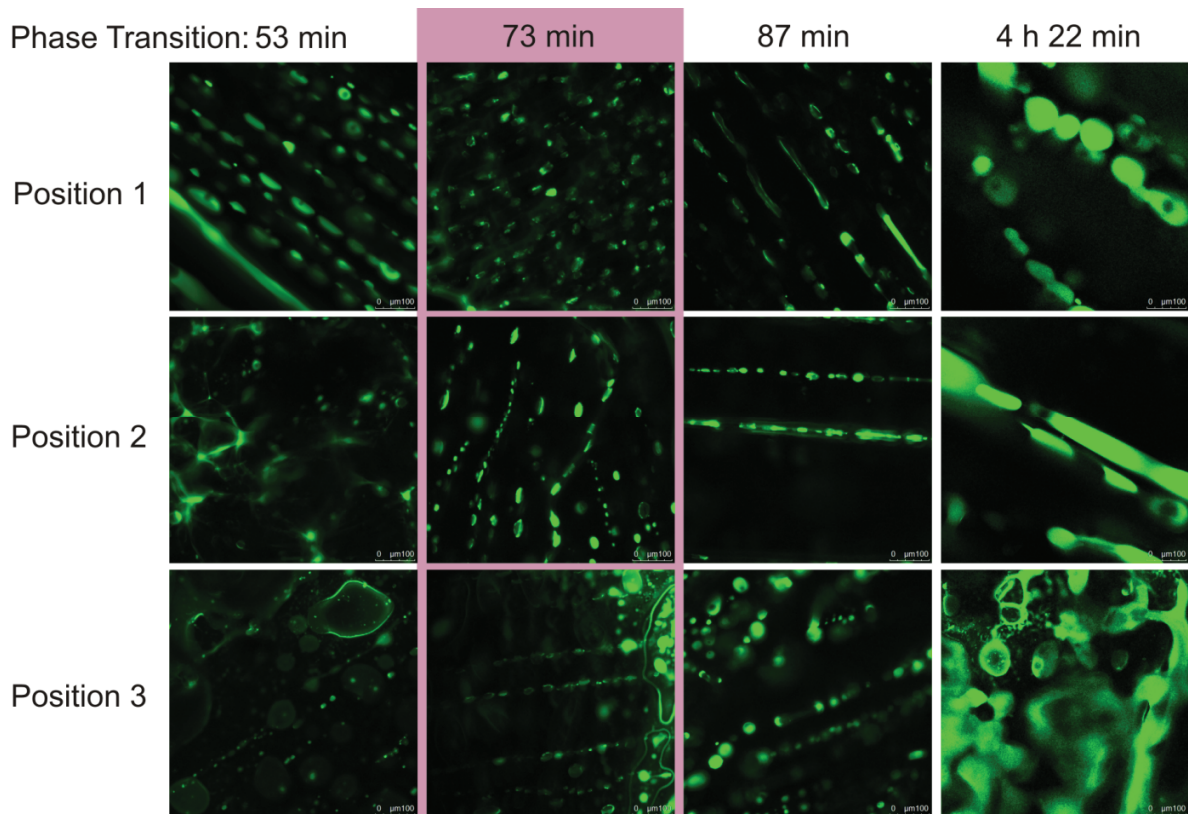


**Figure 2: CLSM images taken from frozen FITC-BSA core samples from positions 1-3 after different freezing protocols yielding different phase transition times. In the highlighted experiment no seeding was performed.**

## ***Discussion***

In all sampling positions we noticed that slower phase transition (87 min, 4 h 22 min) leads to the generation of few, large freeze concentrated regions and wider protein-free regions, except for position 3 (see below). Faster freezing (53 min, 73 min) caused a higher number of smaller freeze-concentrated spots in the ice. Apparently, the fast freezing protocols induced the formation of a high number of small water ice crystals. After nucleation, the different rates of heat removal caused different degrees of supercooling right in front of the growing ice surface. Fast heat removal caused deeper supercooling, more water ice crystals and higher compartmentation. Slow heat removal allowed only a small number of new ice crystals to form which had more time to grow larger and to push labeled BSA molecules from the growing ice surface. The larger freeze-concentrated regions are a result of the higher amount of protein between the larger ice crystals. However, the smallest freeze-concentrated regions were found in position 1, in the experiment with no seeding. Although the overall phase transition time was 73 min the spontaneous nucleation after considerable supercooling caused almost instant solidification of the whole sampling region 1. Also, the linear appearance of the concentrated spots in the other experiments at the same position is not seen there. This alignment could be caused by dendritic ice growth which is often found in bulk-scale freezing. Dendritic growth seems clearly less pronounced when solidification occurs as fast as in the non-seeded case.

In position 3 the overall amount of visible protein is increased as a consequence of macroscopic cryoconcentration. But also the arrangement of concentrated regions becomes more diffuse as position 3 is one of the last points to freeze in the whole container and a unidirectional ice front propagation is no longer the case.

In summary, we established a simple method for the visualization of microscopic cryoconcentration in frozen bulk samples. Using FITC-labeled BSA we showed that cryoconcentration patterns in the microscopic scale are impacted by processing conditions. When phase transition occurs fast a higher number of small cryoconcentrated regions are formed. As this, in turn, is related to increased exposure of protein to ice crystal surfaces, high cooling rates could be unfavorable for freezing of surface-sensitive proteins. With the used method protein concentration differences can be visualized in the frozen state. Further development of the technique might allow protein quantification in the cryoconcentrated regions. Moreover, specialized fluorophores could inform about protein folding or activity in different regions. The established method could thus represent a first step into the better understanding of cryoconcentration and its consequences for frozen protein stability at bulk scales.

## ***Acknowledgements***

Special thanks for CLSM operation go to Heimo Wolinski, Institute of Molecular Biosciences, University of Graz. For financial and technical support and an excellent collaboration thanks go to Zeta Biopharma, especially Birgit Pittermann, Alexander Trausznig, and Karl Muenzer.

This work has been funded within the Austrian COMET Program under the auspices of the Austrian Federal Ministry of Transport, Innovation and Technology (bmvit), the Austrian Federal Ministry of Economy, Family and Youth (bmwfj), and the State of Styria (Styrian Funding Agency SFG). COMET is managed by the Austrian Research Promotion Agency FFG.

## References

1. Singh SK, Nema S. 2010. Freezing and thawing of protein solutions. In *Formulation and process development strategies for manufacturing biopharmaceuticals*; Jameel F, Hershenson S, Eds. Hoboken, New Jersey: JohnWiley & Sons, pp 625–675.
2. Akyurt M, Zaki G, Habeebullah B. 2002. Freezing phenomena in ice–water systems. *Energy Convers Manag.* 43:1773–1789.
3. Kolhe P, Holding E, Lary A, Chico S, Singh SK. 2010. Large-scale freezing of biologics: Understanding protein and solute concentration changes in a cryovessel-part 2. *BioPharm Int.* 23.
4. Rodrigues MA, Miller MA, Glass MA, Singh SK, Johnston KP. 2010. Effect of freezing rate and dendritic ice formation on concentration profiles of proteins frozen in cylindrical vessels. *J Pharm Sci.* 100:1316–1329.
5. Singh S, Kolhe P, Wang W, Nema S. 2009. Large-scale freezing of biologics; A practitioner’s review. Part one: Fundamental aspects. *Bioprocess Int.* 7:32–44.
6. Kolhe P, Badkar A. 2011. Protein and solute distribution in drug substance containers during frozen storage and post-thawing: A tool to understand and define freezing-thawing parameters in biotechnology process development. *Biotechnol Prog.* 27:494–504.
7. Miller MA, Rodrigues MA, Glass MA, Singh SK, Johnston KP, Maynard JA. 2013. Frozen-state storage stability of a monoclonal antibody: Aggregation is impacted by freezing rate and solute distribution. *J Pharm Sci.* 102:1194–1208.
8. Cao E, Chen Y, Cui Z, Foster PR. 2003. Effect of freezing and thawing rates on denaturation of proteins in aqueous solutions. *Biotechnol Bioeng.* 82:684–690.
9. Goding J. 1976. Conjugation of antibodies with fluorochromes: Modifications to the standard methods. *J Immunol Methods.* 13:215–226.
10. Harlow ED, Lane D. 1988. *Antibodies: A laboratory manual.* Cold Spring Harbor, New York: Cold Spring Harbor Laboratory Press. 353–355.
11. Rinderknecht H. 1960. A new technique for the fluorescent labelling of proteins. *Experientia.* 16:430–431.
12. Roessl U, Jajcevic D, Leitgeb S, Khinast JG, Nidetzky B. 2013. Characterization of a laboratory-scale container for freezing protein solutions with detailed evaluation of a freezing process simulation. *J Pharm Sci.* 103:417–426.

## 4 The Impact of Freeze-And-Thaw Processing Conditions on Protein Stability: A Pilot-Scale Study of L-Lactic Dehydrogenase

Ulrich Roessl<sup>1,2</sup>, Seyf Humi<sup>1,2</sup>, Stefan Leitgeb<sup>1</sup>, Bernd Nidetzky<sup>1,2</sup>

*1 Research Center Pharmaceutical Engineering GmbH, Graz, Austria*

*2 Institute for Biotechnology and Biochemical Engineering, Graz University of Technology, Austria*

### **Abstract**

Freezing and thawing of L-lactic dehydrogenase (LDH) in a 700 mL-pilot scale freeze container was investigated. Design of Experiments (DoE) was employed to examine the impact of process parameters on quality attributes of LDH, namely activity, concentration, and aggregation. In 24-hours experiments, storage temperature was found to exert the largest impact on LDH stability with optimal performance at a target temperature of -10°C. Also cooling profile and fill volume showed statistically significant influence on single quality attributes. Established response models allowed for the prediction of quality attributes and thus directed process optimization. Only models related to aggregation responses showed low predictive performance. Exchange of buffer and addition of a surfactant revealed that surface exposure and pH-shift are responsible for poor LDH-stability at lower storage temperatures. We show that the characterization of a freezing and thawing process at intermediate scale can be used to identify process parameters that are critical for the frozen protein's stability. It allows for gaining process controllability and understanding of industrial scale F/T operations at reasonable effort.

## ***Abbreviations***

BSA: Bovine serum albumin, CPP: Critical process parameters, CQA: Critical quality attribute, DoE: Design of experiments, DSC: Differential scanning calorimetry, ECD: Equivalent circular diameter, F/T: Freezing and thawing, LDH: L-lactic dehydrogenase, MLR: Multiple linear regression, QbD: Quality by design,  $T_g'$ : Glass transition temperature of the freeze concentrated matrix.

## ***Introduction***

Storage of bulk volumes of pharmaceutical protein solutions often occurs in the frozen state. In that way, flexibility for manufacturing and distribution is gained for industrial scale volumes of up to several hundred litres.<sup>1</sup> However, substantial losses of high-value product can occur at bulk-scale-conditions.<sup>2-4</sup> F/T studies conducted at mL scale<sup>5</sup> exhibit very limited transferability to the bulk scale. Physical properties differ between the scales. In particular, heat transfer rates with respect to the exchange area, degree of undercooling and cryoconcentration as well as phase transition times vary.<sup>6</sup> Only very few general guidelines can be stated for F/T of proteins at industrial scales.<sup>7</sup> Storage below glass transition temperature ( $T_g$ ) is usually preferred in order to avoid protein aggregation. Above  $T_g$  diffusion is still relevant, and temperature dependence of reaction rates in this regime is even higher than in Arrhenius-type.<sup>8</sup> Below  $T_g$  diffusion is largely attenuated by the high viscosity. Therefore, even if unfolding should occur to some protein molecules they would not act as nuclei for further unfolding or aggregation. Moderate agitation during rapid thawing is considered beneficial for most proteins as this prevents re-crystallization.<sup>1</sup> Yet, only the optimization of F/T processing conditions for each protein can provide stability for the respective formulation. Testing at original scale, however, entails substantial costs through the high amounts of product involved. Intermediate-scale freeze containers thus facilitate process characterization and optimization with acceptable effort but still exhibit characteristics of bulk-scale freezing processes.<sup>3,9,10</sup>

The stability of proteins during F/T and frozen storage is primarily determined by the protein's intrinsic stability towards stresses coming along with the phase transition. Quality attributes, however, can be tuned by altering formulation, e.g. by addition of sugars, polyhydric alcohols, certain amino acids, salts, or surfactants,<sup>7</sup> even though also adverse effects due to precipitation/crystallization effects in the frozen state can be observed.<sup>2</sup> Also the choice of storage buffer can be crucial. Buffer components with different solubility limits during F/T and cryoconcentration might induce substantial pH shifts.<sup>11</sup> Numerous studies confirmed the influence of solution conditions on protein stability,<sup>5,11-14</sup> though most were conducted in volumes not higher than a few millilitres. The influence of F/T process parameters on protein stability at medium (mL to L) or large scale (several L and more) is even less well investigated. Efforts to establish Quality by Design (QbD)-principles throughout pharmaceutical industry, however, expedite deeper investigations of unit processes such as F/T.<sup>15</sup> Profound understanding of underlying biophysical principles, their impact on protein stability and their controllability facilitate total process control and reliable risk management.<sup>16</sup>

A 700 mL stainless steel pilot freeze container was developed in close collaboration with Zeta

Biopharma to enable process-near and QbD-conform investigations of F/T operations at intermediate scale. Process surveillance is possible through four thermocouples and a pH electrode. Filling, emptying, and mixing is done with a peristaltic pump. We investigated the impact of process parameters on the stability of L-lactic dehydrogenase (LDH) during F/T within 24 hours. Due to its sensitivity to F/T-related stresses dilute LDH is useful to indicate the relation of process parameters and protein stability. Design of Experiments (DoE) was applied for statistically balanced variation of process factors to allow for evaluation of their impact on protein quality attributes such as enzymatic activity, soluble protein concentration, and aggregation. Modification of buffer conditions allowed investigation of the LDH inactivation mechanism. We demonstrate that F/T process characterization at pilot scale is crucial for obtaining a reliable control strategy. In that way, identification of critical process parameters and degradation mechanisms using the presented freeze container represent highly valuable tools for a successful scale-up.

## **Materials and Methods**

### Materials

LDH from rabbit muscle in ammonium sulfate suspension and lyophilized bovine serum albumin (BSA) were from Sigma-Aldrich, St. Louis, MO, USA. All other chemicals and reagents used were from Carl Roth GmbH + Co. KG, Karlsruhe, Germany.

PD-10 desalting columns from GE Healthcare, Little Chalfont, UK, were used for buffer exchange.

### Sample preparation

LDH was diluted in 50 mM-sodium phosphate buffer, pH 7.5 to yield a concentration of about 1 mg/mL. After buffer exchange with desalting columns and 0.45 µm-filtration solutions were diluted with the same buffer to 10 µg/mL.

### Design of Experiments

The test panel was designed, and results were analyzed and evaluated using MODDE™ by Umetrics, Umeå, Sweden. A D-optimal experimental design and an interacting model were chosen to screen for critical process parameters (CPP) and critical interactions thereof.<sup>17</sup> *Freezing Time* (1-12 h), *Thawing Time* (1-12 h), *Holding Time* (0-11 h), *Set Temperature* (-10°C,-24°C,-38°C), *Fill Volume* (250 mL, 475 mL, 700 mL), and *Recirculation* of the protein fluid during thawing (Yes or No) were varied. A test panel of 31 experiments, including three center point experiments was generated. (See Supporting Information for experimental details). Specific activity, soluble protein concentration, aggregate number, and mean equivalent circular diameter of aggregates were defined as critical quality attributes (CQA). Contour plots and coefficient plots were also generated with MODDE™.

### Freezing and Thawing

Each F/T experiment lasted 24 hours. *Freezing Time* and *Thawing Time* were defined as the times

for reaching the respective target temperature. Freezing was accomplished by linearly decreasing thermofluid temperature from 20°C to the *Set Temperature* in the period defined as *Freezing Time*. Thawing started 24 hours after experiment start, minus the chosen *Thawing Time*. For thawing the thermofluid temperature was increased linearly to reach 20°C exactly 23 hours after experiment start to assure complete thawing during the last hour.  *Holding Time* was defined as a pre-cooling phase – a part of the *Freezing Time* – with a thermofluid target temperature of -2°C. If a  *Holding Time* was projected, the thermofluid was cooled to -2°C immediately by the start of the experiment. After the  *Holding Time*, the thermofluid temperature was linearly decreased to the final temperature in the rest of *Freezing Time*. For a better comprehension of the F/T protocol design the *Set Temperature* progression of two example runs are plotted in the Supporting Information. *Recirculation* during thawing was accomplished using a peristaltic pump at a speed of 45 mL/min.

#### Response Analytics

An MFI 5100 (Protein Simple, Santa Clara, California) was used for counting and sizing of protein aggregates. Duplicates of 1 mL were measured and averaged. Counting of air bubbles was prevented by applying circularity- and intensity filters. After centrifugation (10 minutes, 18,400 x g) protein concentration was measured as described by Bradford<sup>18</sup> employing Roti-Nanoquant assays (Carl Roth), calibrated with BSA. For the determination of specific LDH activity in centrifuged samples the conversion of 89 mM L-lactate and 4.5 mM NAD<sup>+</sup> to pyruvate and NADH (TRIS buffer, 50 mM, pH 8) was followed spectrophotometrically at 340 nm and 37°C (Beckman Coulter DU 800 spectrophotometer).  $T_g'$  was determined by differential scanning calorimetry (DSC) on a DSC 204 F1 Phoenix<sup>TM</sup>, equipped with a  $\mu$ -Sensor and an intracooler (Netzsch, Selb, Germany). Triplicate DSC-measurements were performed at a heating rate of 40 K/min.

#### pH Monitoring

pH during F/T was measured using an InPro 3251 electrode attached to an M400 transmitter by Mettler-Toledo (Greifensee, Switzerland). Values were recorded via an NI 9203 current input module and LabView<sup>TM</sup> software (National Instruments, Austin, Texas). Calibration was performed at room temperature.

## Freezer design

The Zeta pilot freezer allows investigation of bulk freezing effects in a moderate volume, up to 700 mL, with online-monitoring of the bulk temperature at up to four positions. A system overview is shown in Figure 1. Material properties of the stainless steel vessel (AISI316L - 1.4435/1.4404, Ra < 0.8  $\mu\text{m}$ ) are the same as in the commercial 300 L Freeze Container by Zeta Biopharma GmbH, Lieboch, Austria. The jacket and the cooling coils inside the vessel are cooled by the thermofluid which is circulated and cooled by an external freeze controller (Tango Nuevo thermostat by Peter Huber Kaeltemaschinenbau GmbH, Offenburg, Germany). Silicone oil (M40.165.10 by Huber) was used as thermofluid. Process temperatures were measured with an 8-channel PCE-T 800 multi-input thermometer. Sample temperature was  $20 \pm 1^\circ\text{C}$  at the start. The thermofluid was equilibrated for 10 min to  $20^\circ\text{C}$ . No seeding was performed to ensure process-near conditions.



**Figure 1: Pilot freeze container system overview; external freeze controller is not shown.**

## Results and Discussions

### DoE and Response Modelling

The aim of the present work was to evaluate the impact of F/T-process parameters CQAs of a model protein. Furthermore, we were interested if F/T-process design is actually crucial, and to what extent a process can be characterized and optimized on a pilot-scale level. We chose process parameters that were found to influence stability of other proteins and that were controllable also at larger scales (Note that the shown process is not an actual scale-down of processes in larger freezing containers). By choosing an experiment duration of only 24 hours we emphasize the freezing and thawing phases compared to the storage period. Maximum and minimum of the process parameters were defined with the total experiment duration of 24 hours and the temperature minimum achievable with the cooling unit, respectively. The pump flow rate was chosen in order to assure adequate mixing and yet to avoid foam formation by harsh agitation. Specific enzymatic activity, solubility-, and aggregation values were chosen as CQAs as they allow generic estimation of protein stability. Also, these measures are easily accessible even for very low LDH concentrations.

**Table 1: Brief descriptive statistics of response results and properties of MLR fitting for each response.**

	Min	Max	Mean	N	R2	Q2	Reproducibility	Model Validity
Specific Activity (%)	0.0	94	34	30	0.83	0.67	0.73	0.88
Soluble Protein Concentration (%)	21	87	45	30	0.80	0.49	0.64	0.89
Aggregate Concentration ( $10^4$ /ml)	1.0	11.0	4.6	30	0.49	0.31	0.04	0.94
Mean Aggregate Size ( $\mu\text{m}_{\text{ECD}}$ )	2.7	5.1	3.8	30	0.73	0.33	0.80	0.75

Of the 31 scheduled experiments, the one with a combination of highest *Set Temperature* and *Freezing Time* did not qualify for further analysis. The plateau in the bulk temperature profile was not complete after *Freezing Time*, indicating that the solution was not totally frozen. The other 30 experiments were performed successfully. CQA values of each run can be found in the Supporting Information. Brief descriptive statistics of the DoE-screening are shown in Table 1. For each response, model generation was done using multiple linear regression (MLR) in MODDE™. Parameters or parameter interactions were removed from the models, if, according to MODDE™-generated coefficient plots, no statistically significant impact on CQAs and model quality was

found. Coefficient plots are displayed in the Supporting Information. Table 1 shows fitting properties for each response. Among the responses, only aggregate number exhibits unsatisfactory model quality, due to the high variation found in repeated experiments and the low variation explained by the model. Therefore, the significance of predictions and coefficients derived from that model is expected to be low.

In the following sections we describe the screening results for each response, separately:

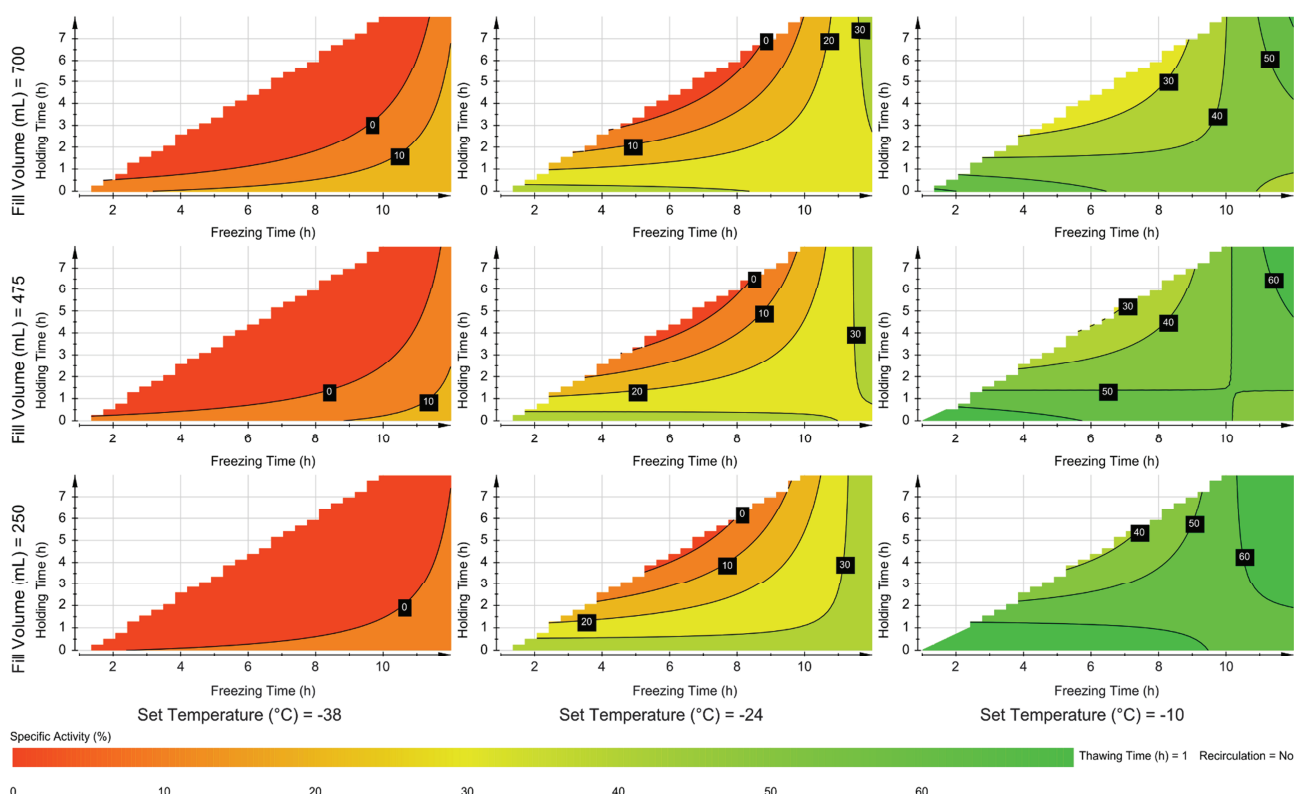


**Figure 2: Impact of selected process parameters on specific LDH activity retention after 24 hours F/T.**

### Specific LDH Activity

A very broad range of specific activity retention between 0 and 94 % was observed in screening experiments. *Set Temperature* and *Freezing Time* were found to have significantly positive, while *Holding Time* showed significantly negative impact. Only in connection with high *Freezing Time*, also high *Holding Time* is preferred due to an interactive positive effect on specific activity. This complex interplay of CQAs and CPPs can be visualized comprehensively using contour plots. Also,

the existence of non-linear effects can be verified easily in that way. Figure 2 can be used to conveniently identify regions in the design space where high activity retention can be expected. For instance, higher *Set Temperature* is clearly beneficial for activity retention whereas *Holding Time* is only advantageous in combination with higher *Freezing Time*.

### Soluble Protein Concentration

The most influential parameter for soluble protein concentration was again *Set Temperature*, exhibiting a clear positive correlation. Due to interactive effects also *Freezing Time* and *Holding Time* show a minor impact on soluble protein concentration (Figure 3). In screening experiments we found protein concentration values between 21 and 87 % (Table 1).

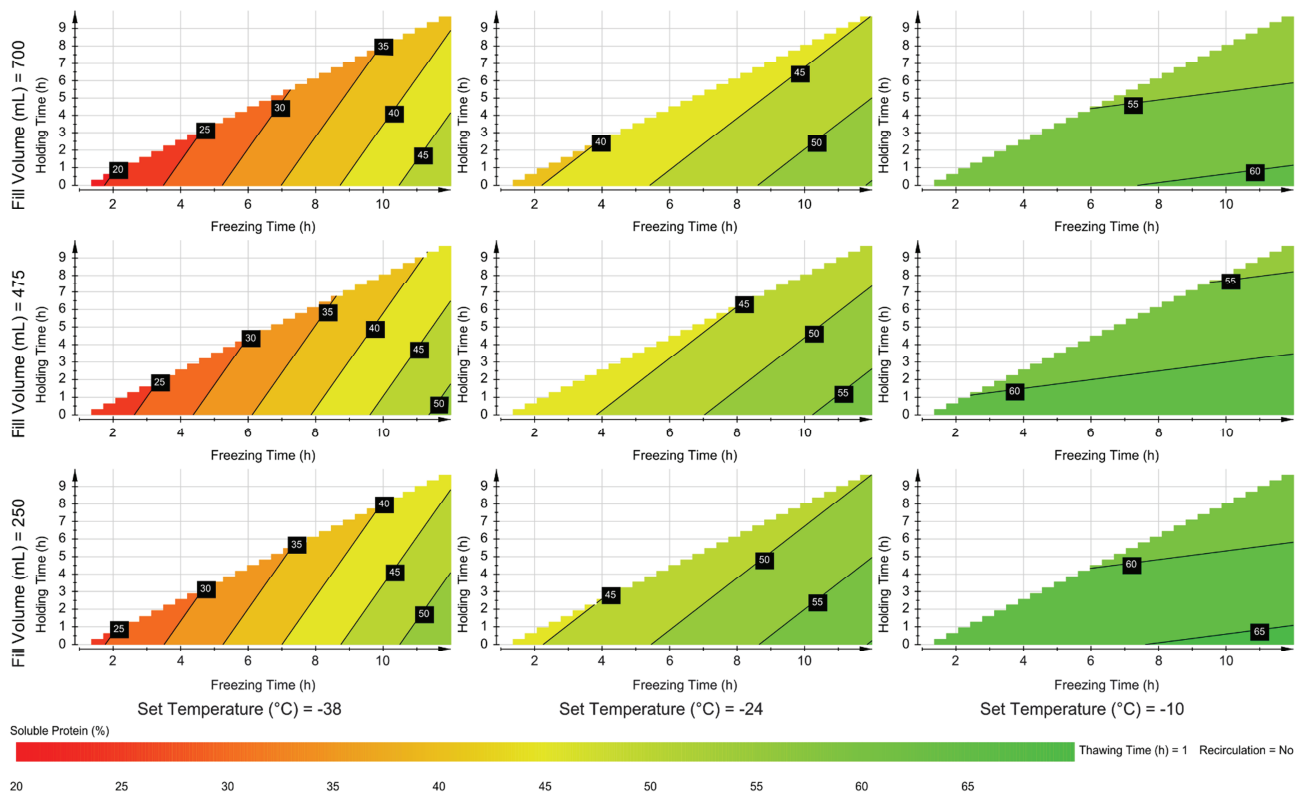


**Figure 3: Impact of selected process parameters on soluble LDH concentration after 24 hours F/T.**

## Aggregate Concentration

High variability of aggregate concentration values was observed, ranging over one order of magnitude (Table 1). Due to the low reproducibility fitting was difficult, and only *Set Temperature* could be identified as significantly critical parameter with a negative correlation (Figure 4). *Thawing Time* and *Fill Volume* were found to have small interactive impact.

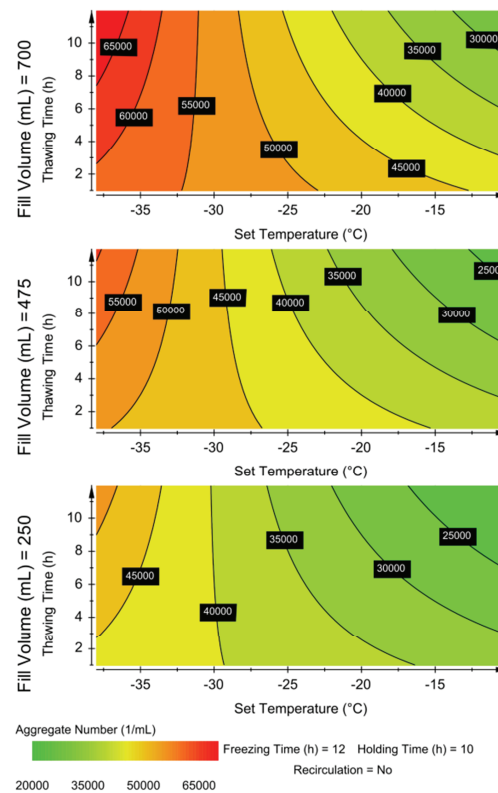


**Figure 4: Impact of selected process parameters on LDH aggregate concentration after 24 hours F/T.**

## Mean Aggregate Size

Aggregate size varied between 2.7 and 5.1  $\mu\text{m}_{\text{ECD}}$  (Table 1). Mean values might not sufficiently describe aggregate distributions. Nonetheless, we decided to use mean aggregate size as single number enabling simple discrimination of distributions.

*Fill Volume* was the only single parameter with a significantly positive impact on aggregate size. However, due to an interactive effect together with *Freezing Time* also *Set Temperature* appears critical according to the contour plot in Figure 5.

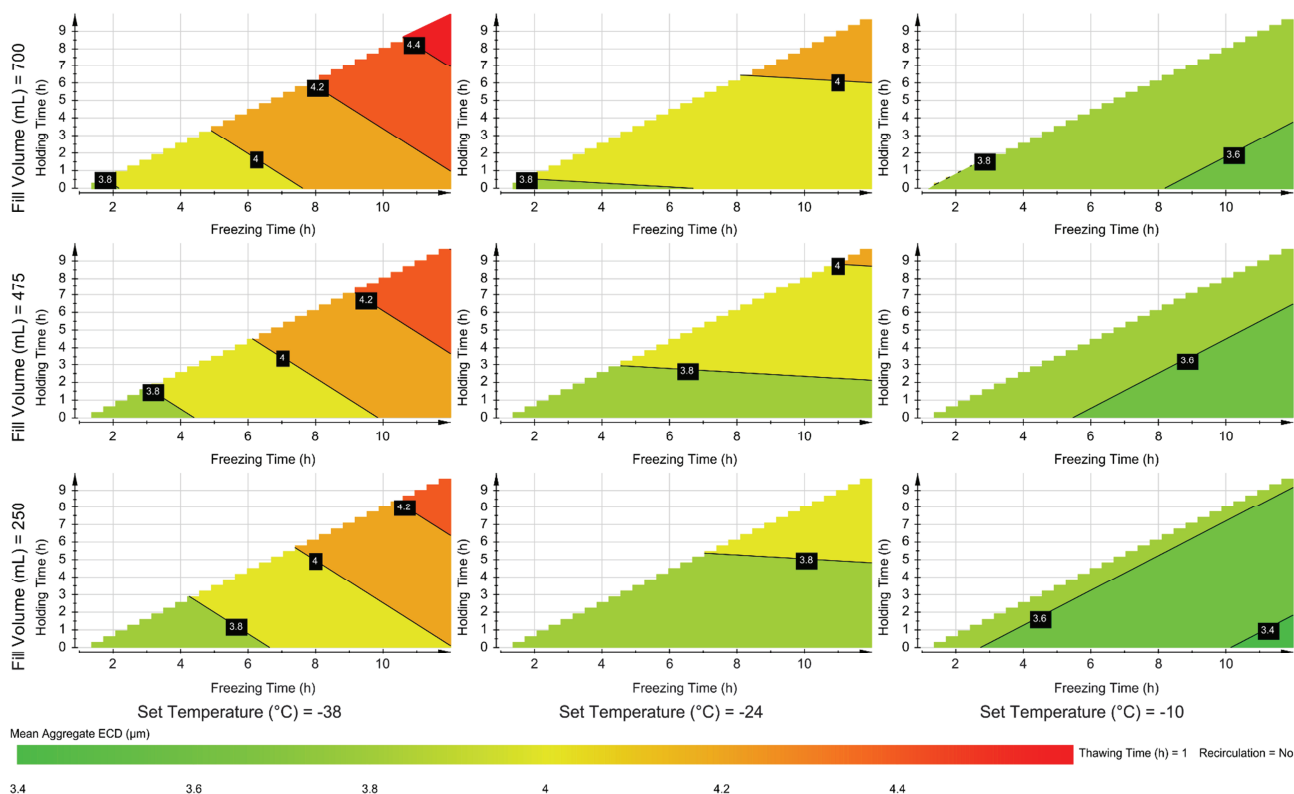


**Figure 5: Impact of selected process parameters on mean LDH aggregate size after 24 hours F/T.**

### Evaluation of CPPs

As mentioned above, *Set Temperature* had statistically significant impact on 3 of 4 responses. Also *Freezing Time*, *Holding Time*, and *Fill Volume* showed impact on one response. Among interactive effects, *Freezing Time/Set Temperature* is the only one with an effect on multiple responses, which are specific activity, soluble protein concentration and aggregate size. For the other parameters – *Thawing Time* and *Recirculation* – only few interactive effects of low significance could be detected.

Therefore, only *Set Temperature*, *Freezing Time*, *Holding Time*, and *Fill Volume* are relevant factors for the present F/T process. Knowing that, it was possible to build the design space in regard to the identified CPPs. Within the design space a region with desirable response values can be defined. Using the response models it should be possible to establish control strategies to keep CQAs within this operation space. For the current process, operations would be restricted to very slow freezing to rather high temperatures. The usability of the models for that purpose was eventually evaluated as

presented below

All identified CPPs (*Set Temperature*, *Freezing Time*, *Holding Time*, *Fill Volume*) are related to the freezing operation while the thawing-related parameters, *Thawing Time* and *Recirculation*, exert no influence. Therefore, disregarding the length of the storage period, the degree of damage to LDH is defined when freezing is completed. Conclusions about underlying inactivation mechanisms, however, can not be drawn solely from screening experiments and shall be evaluated later. In this special case, freezing might not seem to be advisable for LDH-storage. Still, LDH-freezing represents a showcase for the applicability of pilot scale freezing and QbD for process characterization and optimization, and thus aided argumentation for investigations at intermediate scales.

#### Response model validation

Based on screening results validation experiments were designed to assess predictive quality of the models. Process parameters and results are displayed in Table 2. The parameters for run A, B, and C were compiled using the optimizer function of MODDE™ to yield highest response values for all CQAs. Run X, Y, and Z were designed manually to provide also negative scenarios for the validation. Non-critical parameters, according to the screening results, were fixed at a beneficial or practical level: *Recirculation* was stalled, *Thawing Time* was set to 1 hour, and *Fill Volume* was set to 700mL. Although *Fill Volume* was found to slightly increase aggregate size we decided to further investigate conditions for maximal *Fill Volume* as this seemed more efficient and realistic than minimizing the *Fill Volume*.

The three optimized experiments (A, B, C) were performed at relatively high *Set Temperature* with varying *Freezing Time*. The non-optimized experiments (X, Y, Z) were particularly designed to exhibit low *Set Temperature* while yielding poor predictions from the response models.

Validation results for the optimized experiments (A, B, C) showed increased levels of soluble protein concentration and specific activity compared to the non-optimized runs (X, Y, Z). Aggregation parameters however showed no differences (Table 2).

Therefore, the established response models can partially be applied for the prediction and optimization of response levels for the investigated F/T process. For soluble protein concentration and specific activity, response models adequately predicted responses values. Modelling of aggregation values was more difficult. Especially aggregate number yielded poor model properties.

Hence, the models for aggregate number and aggregate size could not be used for an accurate prediction of responses under defined process parameters. It appears that the effects of the investigated process parameters were overestimated by our models and that other, untested parameters had a higher influence on the aggregation-related responses. Above others, those untested parameters might include the time point of nucleation. Seeding was not performed in the current setting as it is not possible in the industrial case, either. However, by avoiding supercooling it would have rendered the phase transition time more controllable and higher reproducibility of aggregation responses might have been reached. Also, a relationship between process parameters and responses, more complex than expected through regression modelling with MODDE™ could be a reason for the poor predictive performance of the aggregation models. Broader and/or higher resolved screening of the design space for CPPs, probably in a full-factorial design, would be necessary for an appropriate model refinement.

**Table 2: Parameters and results of validation experiments. A-C: Parameters designed using the MODDE™ optimizer-tool for improved freezing performance; X-Z: experiments manually designed for poor performance; predicted values derived from response models established after DoE. Fill Volume = 700 mL, Thawing Time = 1 h, No Recirculation.**

Run	Freezing Time (h)	Holding Time (h)	Set Temperature (°C)	Soluble Protein Concentration (Predicted) (%)	Soluble Protein Concentration (Measured) (%)	Specific Activity (Predicted) (%)	Specific Activity (Measured) (%)	Aggregate Number Predicted (10 <sup>6</sup> /mL)	Aggregate Number Measured (10 <sup>6</sup> /mL)	Mean Aggregate Size Predicted (μm <sub>ECD</sub> )	Mean Aggregate Size Measured (μm <sub>ECD</sub> )
A	1	0	-10.0	58	71	62	58	4.4	4.6	3.8	4.0
B	4	0	-11.7	57	67	53	67	4.5	4.6	3.7	3.8
C	12	8	-10.0	53	70	61	83	4.4	5.1	3.7	3.9
X	6.5	5	-24.0	41	62	0	25	5.2	5.5	4.0	3.8
Y	12	0	-30.0	53	42	23	19	5.5	4.3	4.1	3.5
Z	12	0	-34.0	51	62	20	22	5.7	3.5	4.2	4.1

#### Evaluation of LDH-inactivation mechanism

From screening and model evaluation we found that storage at higher temperatures provides higher LDH stability during the 24 hours-experiments. This was somehow unexpected as usually lower storage temperatures are preferred. It is commonly accepted that frozen storage should occur at temperatures below  $T_g'$ . Especially for long term storage periods, protein solutions stored above  $T_g'$  are more prone to show aggregation due to higher mobility of proteins in the freeze-concentrated regions.<sup>1</sup> However, for the investigated liquid we measured a  $T_g'$  of  $-27.3 \pm 0.7^\circ\text{C}$ .

One explanation for higher stability retention at higher temperatures could be cold denaturation which has already been observed for LDH at temperatures of around  $-28^{\circ}\text{C}$ .<sup>19,20</sup> Cold denaturation could lead to conformational destabilization. This, in turn, could increase probability of unfolding due to surface stresses, for instance. Surface stresses per se could also be responsible for LDH inactivation at lower temperatures, as suggested before.<sup>21</sup> Sodium phosphate buffer is known to exhibit a substantial pH-shift in the frozen state due to early precipitation of  $\text{Na}_2\text{HPO}_4 \cdot 12\text{H}_2\text{O}$ .<sup>22,23</sup> Thus, the exposure to lower pH might also cause LDH-inactivation.<sup>24</sup>

In additional F/T experiments we investigated the mechanism underlying LDH-inactivation at lower temperatures. We established a freezing procedure which allowed examining the effect of temperature alone. The thermofluid temperature was first set to  $-20^{\circ}\text{C}$  for 2 hours, followed by further cooling to the final *Set Temperature* ( $-20^{\circ}\text{C}$ ,  $-25^{\circ}\text{C}$ ,  $-30^{\circ}\text{C}$ ,  $-35^{\circ}\text{C}$ ). In this way, the conditions during phase transition were the same for all runs. Testing whether a pH-shift is responsible for inactivation was done by replacing sodium phosphate buffer with 50 mM Tris-HCl buffer (pH 7.5 at room temperature) and freezing to *Set Temperature* =  $-30^{\circ}\text{C}$  as just described. The development of pH was monitored during these experiments. The possibility of inactivation due to surface effects should be eliminated by the addition of 0.02% of the non-ionic surfactant Tween™ 80 during freezing to  $-30^{\circ}\text{C}$  the same way.<sup>25</sup> Other process parameters remained the same as during the optimization experiments.

A sudden drop in specific activity was the result of adjusting *Set Temperature* to below  $-20^{\circ}\text{C}$ , which corresponds to an inner bulk temperature of  $-14.4^{\circ}\text{C}$  (Table 3). Also aggregate number and size showed a trend to increased levels below that point while protein concentration showed no clear tendency. However, we found that bulk temperatures up to about  $-14.4^{\circ}\text{C}$  impair particularly LDH activity, but also promote aggregation. We can further affirm that these effects are not related to the phase transition during freezing or thawing. They are alone consequences of the temperature during frozen storage.

**Table 3: Evaluation of temperature influence on LDH inactivation during frozen storage. Total experiment = 24 h, Holding Time at  $-20^{\circ}\text{C}$  = 2 h, Fill Volume = 700 mL, Thawing Time = 1 h, No Recirculation.**

Run	Set Temperature ( $^{\circ}\text{C}$ )	Bulk Temperature ( $^{\circ}\text{C}$ )	Protein Concentration (%)	Specific Activity (%)	Aggregate Number ( $10^4/\text{mL}$ )	Aggregate Size ( $\mu\text{m}_{\text{ECD}}$ )
1	-20	-14.4	58	68	4.0	3.5
2	-25	-17.8	46	19	5.6	4.0
3	-30	-21.0	75	19	11.0	3.5
4	-35	-25.9	69	15	5.3	3.9

While the use of sodium phosphate buffer caused a pH shift to  $3.6 \pm 0.1$ , the pH in Tris-HCl buffer

remained neutral during the whole F/T procedure (Figure 6C). This alone led to significant improvement of activity retention and aggregation (Figure 6, panel A and B). Surface stress reduction by Tween™ 80-addition alone did not improve these responses, the performance was even worse. Only a combination of buffer exchange and surfactant addition led to further significant improvement of F/T performance to a specific activity of  $84.0 \pm 5.3$  % and an aggregate count of  $0.6 \pm 0.2$   $10^4$ /mL. No significant improvement due to Tris-HCl buffer or Tween™ 80 was found for soluble protein concentration and aggregate size.

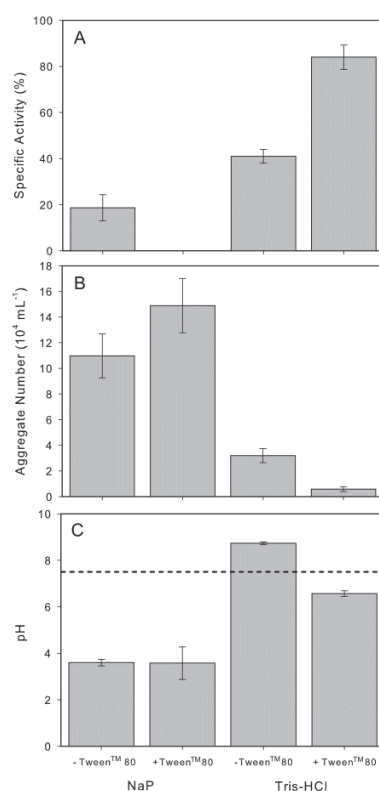


**Figure 6: Effects of pH stabilization and Tween™ 80 addition in F/T experiments on specific activity (A), aggregate number (B) and frozen-state pH (C). Dashed line represents initial pH at RT. Total experiment = 24 h, Holding Time at  $-20^{\circ}\text{C}$  = 2 h, Fill Volume = 700 mL, Thawing Time = 1 h, No Recirculation.**

However, poor LDH stability due to lower temperatures was confirmed, while LDH can be stabilized by the combination of Tris-HCL buffer and surfactant addition. This suggests that predominantly precipitation of  $\text{Na}_2\text{HPO}_4 \cdot 12\text{H}_2\text{O}$  and/or its concomitant pH drop in the frozen state is responsible for the observed behavior.

The pH drop to 3.6 persisted during storage when the inner bulk temperature was clearly below a temperature of  $-14^{\circ}\text{C}$  to  $-17^{\circ}\text{C}$ . Above that temperature range a pH drop was only observed temporarily during solidification. In the storage phase a neutral pH was re-established. For bulk

temperatures between  $-14^{\circ}\text{C}$  and  $-17^{\circ}\text{C}$  the persistence of the pH shift seemed more related to the freezing rate than to the final temperature, though clear relations could not be confirmed.

In sodium phosphate buffer a  $T_g'$  was measured at  $-27.3 \pm 0.7^{\circ}\text{C}$  for LDH. Diffusion should be halted below that temperature, while above certain diffusive mobility is possible in the frozen bulk. However, due to our results we can conclude that storage even at temperatures of up to  $-17^{\circ}\text{C}$  confines diffusive mobility in freeze-concentrated regions. It seems low enough to prevent dissolution of precipitated  $\text{Na}_2\text{HPO}_4 \cdot 12\text{H}_2\text{O}$  and recovery of pH. Above that temperature range mobility is high enough for  $\text{Na}_2\text{HPO}_4 \cdot 12\text{H}_2\text{O}$  to dissolve (after initial precipitation during solidification) and for the pH to neutralize. As this is apparently not the case below that critical temperature range, LDH is exposed to precipitated  $\text{Na}_2\text{HPO}_4 \cdot 12\text{H}_2\text{O}$  and low pH during the whole storage period. Then, inactivation occurs, most probably through LDH subunit dissociation followed by aggregation.<sup>12,26</sup> The involvement of cold denaturation in the observed LDH inactivation behavior could not be confirmed in this set-up. Temperatures at which cold denaturation was observed for LDH were described to lie well below the investigated critical temperature threshold. Thus, it is unlikely that cold denaturation contributes to LDH inactivation. However, the relevance of cold denaturation cannot be totally excluded since observations of LDH cold denaturation occurred in matrices different from the present.

## Conclusions

Employing a 700 mL pilot-scale freeze container we investigated critical parameters of a F/T process. DoE-based screening followed by response modelling was employed to determine the impact of CPPs on quality attributes of LDH. *Set Temperature* was identified as the most critical parameter for LDH stability. A *Set Temperature* of -10°C provided the highest F/T performance for LDH while only poor LDH stability was observed at a *Set Temperature* of -38°C. As adverse effects of low temperatures could be minimized by avoiding sodium phosphate buffer and adding Tween™ 80, LDH degradation could be related to its exposure to precipitated  $\text{Na}_2\text{HPO}_4 \cdot 12\text{H}_2\text{O}$  and the conjoint pH drop when mobility in the freeze-concentrated matrix was too low for an equilibration during storage. Also *Freezing Time*, *Holding Time* (at -2°C) and *Fill Volume* had a significant impact on CQAs in a way that slow phase transition was preferred for higher LDH stability. With regard to the temperature dependence of LDH inactivation this is probably due to the reduced net storage time with exposure to surface stress and low pH. However, the fact that *Thawing Time* did not show an impact on CQAs at all might also suggest that slow solidification itself is preferred. Slow solidification usually leads to higher macroscopic cryoconcentration. This in turn could exert cryoprotective effects on diluted LDH, as suggested by earlier work from this group.<sup>10</sup> Agitation during thawing using a peristaltic pump had no effect on LDH stability.

The response models for protein concentration and specific activity were successfully validated and applied to process optimization by response prediction. Validation of models for aggregation responses failed. Controlled ice nucleation by seeding and/or broader/more detailed evaluation of critical parameters could further improve model quality. Yet, by the use of a pilot freeze container it was possible to characterize an LDH-F/T process at moderate cost and time. Both, an empiric optimization strategy as well as deeper investigations of the underlying inactivation mechanism were performed with respect to QbD principles. Though LDH with its sensitivity towards F/T<sup>5</sup> might represent an untypical model protein the presented approach can be applied to characterize and optimize F/T processes of various pharmaceutical protein preparations at different scales. The unexpected inactivation behaviour of LDH underlines the necessity of pilot-scale F/T experiments, rendering them an important handle for the reasonable determination of the best storage conditions of pharmaceutical proteins.

## ***Acknowledgements***

For financial and technical support and an excellent collaboration thanks go to Zeta Biopharma, especially Birgit Pittermann, Alexander Trausznig, and Karl Muenzer. From Research Center Pharmaceutical Engineering we thank Otto Scheibelhofer for assistance with DoE and Mario Hainschitz for DSC measurements. Furthermore, for continuous help and advice we want to thank Satish Singh, Pfizer Inc.

This work has been funded within the Austrian COMET Program under the auspices of the Austrian Federal Ministry of Transport, Innovation and Technology (bmvit), the Austrian Federal Ministry of Economy, Family and Youth (bmwfj), and the State of Styria (Styrian Funding Agency SFG). COMET is managed by the Austrian Research Promotion Agency FFG.

## References

1. Singh S, Kolhe P, Wang W, Nema S. 2009. Large-scale freezing of biologics; A practitioner's review. Part one: Fundamental aspects. *Bioprocess Int.* 7:32–44.
2. Singh SK, Kolhe P, Mehta AP, Chico SC, Lary AL, Huang M. 2011. Frozen state storage instability of a monoclonal antibody: Aggregation as a consequence of trehalose crystallization and protein unfolding. *Pharm Res.* 28:873–885.
3. Radmanovic N, Serno T. 2013. Understanding the freezing of biopharmaceuticals: First principle modeling of the process and evaluation of its effect on product quality. *J Pharm Sci.* 102:2495–2507.
4. Miller MA, Rodrigues MA, Glass MA, Singh SK, Johnston KP, Maynard JA. 2013. Frozen-state storage stability of a monoclonal antibody: Aggregation is impacted by freezing rate and solute distribution. *J Pharm Sci.* 102:1194–1208.
5. Nema S, Kenneth E. 1993. Freeze-thaw studies of a model protein, lactate dehydrogenase, in the presence of cryoprotectants. *PDA J Pharm Sci.* 47:76–83.
6. Singh SK, Nema S. 2010. Freezing and thawing of protein solutions. In *Formulation and process development strategies for manufacturing biopharmaceuticals*; Jameel F, Hershenson S, Eds. Hoboken, New Jersey: JohnWiley & Sons, pp 625–675.
7. Singh SK, Kolhe P, Wang W, Nema S. 2009. Large-scale freezing of biologics; A practitioner's review. Part two: Practical advice. *Bioprocess Int.* 7:34–42.
8. Schenz TW. 1995. Glass transitions and product stability—an overview. *Food Hydrocoll.* 9:307–315.
9. Shamlou PA, Breen LH, Bell WV, Pollo M, Thomas BA. 2007. A new scaleable freeze-thaw technology for bulk protein solutions. *Biotechnol Appl Biochem.* 46:13–26.
10. Roessl U, Jajcevic D, Leitgeb S, Khinast JG, Nidetzky B. 2013. Characterization of a laboratory-scale container for freezing protein solutions with detailed evaluation of a freezing process simulation. *J Pharm Sci.* 103:417–426.
11. Pikal-Cleland K. 2000. Protein denaturation during freezing and thawing in phosphate buffer systems: Monomeric and tetrameric  $\beta$ -galactosidase. *Arch Biochem Biophys.* 384:398–406.
12. Anchordoquy TJ, Carpenter JF. 1996. Polymers protect lactate dehydrogenase during freeze-drying by inhibiting dissociation in the frozen state. *Arch Biochem Biophys.* 332:231–238.
13. Tamiya T, Okahashi N, Sakuma R. 1985. Freeze denaturation of enzymes and its prevention with additives. *Cryobiology.* 456:446–456.
14. Bhatnagar BS, Bogner RH, Pikal MJ. 2007. Protein stability during freezing: separation of stresses and mechanisms of protein stabilization. *Pharm Dev Technol.* 12:505–523.

15. Rathore A, Winkle H. 2009. Quality by design for biopharmaceuticals. *Nat Biotechnol.* 27: 26-34.
16. Stability testing of new drug substances and products. 2003. Guideline, ICH Harmonised Tripartite. Topic Q1A (R2).
17. Eriksson L, Johansson E, Kettaneh-Wold N, Trygg J, Wikström C, Wold S. Multi-and megavariate data analysis: Part I: Basic principles and applications. Umeå, Sweden: Umetrics AB.
18. Bradford MM. 1976. A rapid and sensitive method for the quantitation of microgram quantities of protein utilizing the principle of protein-dye binding. *Anal Biochem.* 72:248–254.
19. Hatley RH, Franks F. 1989. The cold-induced denaturation of lactate dehydrogenase at sub-zero temperatures in the absence of perturbants. *FEBS Lett.* 257:171–173.
20. Franks F. 1995. Protein destabilization at low temperatures. *Adv Protein Chem.* 46:105–139.
21. Bhatnagar B, Pikal M, Bogner RH. 2008. Study of the individual contributions of ice formation and freeze concentration on isothermal stability of lactate dehydrogenase during freezing. *J Pharm Sci.* 97:798–814.
22. Gomez G, Pikal MJ, Nair R-H. 2001. Effect of initial buffer composition on pH changes during far-from-equilibrium freezing of sodium phosphate buffer solutions. *Pharm Res.* 18:90–97.
23. Van Den Berg L, Dyson R. 1959. Effect of freezing on the pH and composition of sodium and potassium phosphate solutions: the reciprocal system  $\text{KH}_2\text{PO}_4\text{-Na}_2\text{HPO}_4\text{-H}_2\text{O}$ . *Arch Biochem Biophys.* 81:319–329.
24. Zheng Y, Guo S, Guo Z, Wang X. 2004. Effects of N-terminal deletion mutation on rabbit muscle lactate dehydrogenase. *Biochemistry (Moscow).* 69(4)401–406.
25. Hillgren A, Lindgren J, Aldén M. 2002. Protection mechanism of tween 80 during freeze-thawing of a model protein, LDH. *Int J Pharm.* 237:57–69.
26. Pikal-Cleland KA, Cleland JL, Anchordoquy TJ, Carpenter JF. 2002. Effect of glycine on pH changes and protein stability during freeze–thawing in phosphate buffer systems. *J Pharm Sci.* 91:1969–1979.

## Supporting Information

**Table S1: DoE-derived test panel for screening for critical process parameters of a 24-hours F/T process as described in the main article.**

Run Order	Freezing Time (h)	Thawing Time (h)	Holding Time (h)	Fill Volume (mL)	Set Temperature (°C)	Recirculation (Yes/No)	Soluble Protein Concentration (%)	Specific Activity (%)	Aggregate Number (10 <sup>4</sup> /mL)	Mean Aggregate Size (µm <sub>ECD</sub> )
1	12	12	10	700	-10	No	65.8	55.3	2.4	3.5
2	12	1	10	250	-38	Yes	48.3	13.2	4.3	3.2
3	12	12	0	250	-10	No	67.9	62.6	1.0	3.3
4	1	12	0	700	-38	No	35.1	0	8.3	4.6
5	1	12	0	250	-38	Yes	22.4	24	3.2	2.7
6	12	1	10	700	-10	Yes	43.8	69.9	4.4	4.1
7	12	1	0	250	-10	No	65.5	64.0	2.9	3.6
8	12	12	10	250	-38	No	42.9	17.8	5.2	4.3
9	12	12	0	700	-38	Yes	44.4	47.0	5.7	3.5
10	12	12	10	250	-10	Yes	23.3	75.6	1.4	3.8
11	1	1	0	700	-38	Yes	21.2	44.8	6.8	3.7
12	12	1	0	700	-10	Yes	32.5	29.6	6.6	4.3
13	12	1	0	250	-38	Yes	40.4	26.1	4.5	3.4
14	1	1	0	700	-10	No	62.7	76.9	2.7	3.9
15	6.5	6.5	5	475	-24	Yes	45.5	1.8	3.3	3.7
16	1	1	0	250	-38	No	27.4	0.0	5.0	3.5
17	12	1	10	250	-10	No	55.6	93.8	3.0	3.6
18	1	12	0	700	-10	Yes	61.2	58.3	3.0	4.6
19	12	1	0	700	-38	No	55.7	28.4	3.3	4.0
20	12	12	0	250	-38	No	40.8	12.4	7.4	3.9
21	1	1	0	250	-10	Yes	59.4	68.9	2.7	3.6
22 <sup>a</sup>	12	12	0	700	-10	No	-	-	-	-
23	6.5	6.5	0	475	-24	No	39.5	0.0	4.7	3.5
24	12	1	10	700	-38	No	35.3	0.0	5.2	4.5
25	1	12	0	250	-10	No	52.9	71.6	3.3	3.6
26	12	12	10	700	-38	Yes	57.4	29.5	5.7	5.1
27	8.3	6.5	3.3	475	-24	No	33.7	0.0	7.3	4.1
28	6.5	6.5	5	475	-24	No	43.9	0.0	4.9	3.9
29	12	6.5	5	475	-24	Yes	37.5	14.3	11	4.2
30	8.3	6.5	3.3	475	-24	No	48.8	26.1	2.7	4.2
31	8.3	6.5	3.3	475	-24	No	36.5	0.0	5.1	3.8

<sup>a</sup> Experiment not used for analysis due to incomplete freezing

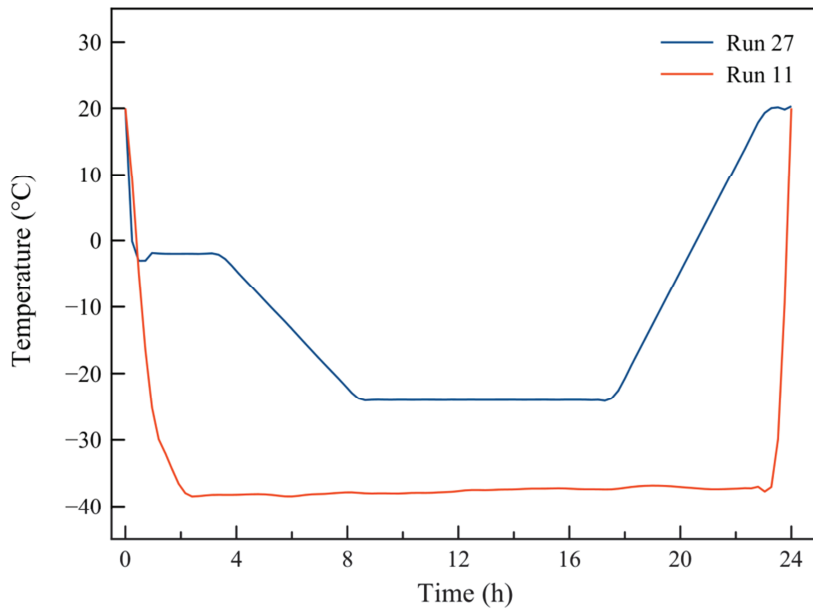


**Figure S1: Thermofluid temperature progression of two example screening runs to illustrate the design of F/T protocols. Run 11: Freezing Time: 1 h, Thawing Time: 1 h. Run 27: Freezing Time: 8.3 h, Holding Time: 3.3 h, Thawing Time: 6.5h**

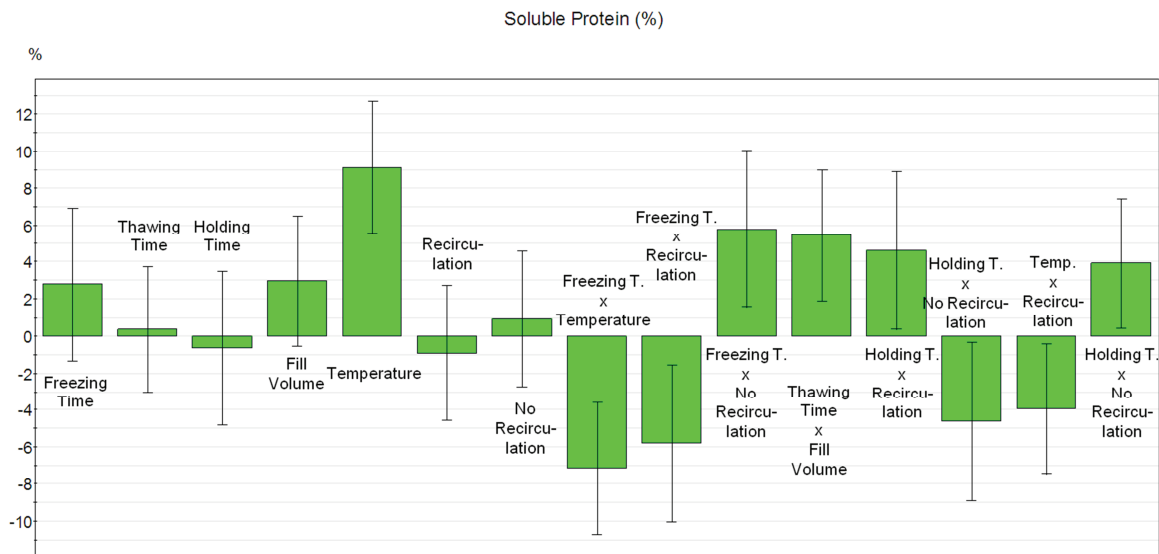


**Figure S2: Coefficient plot for soluble protein concentration model derived from DoE-screening; scaled and centered, confidence level 95 %.**

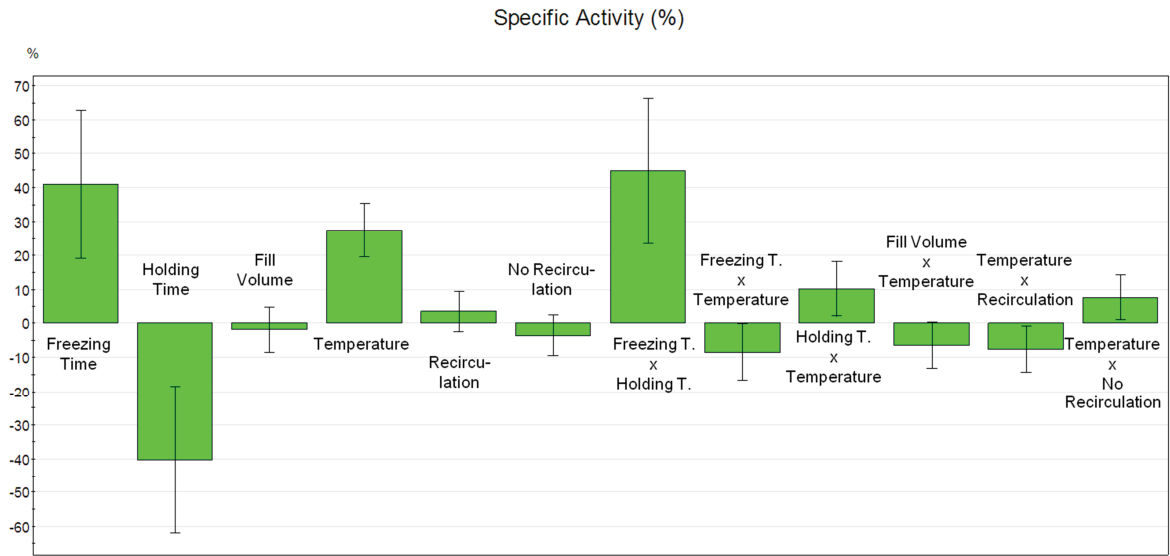


Figure S3: Coefficient plot for specific LDH activity model derived from DoE-screening; scaled and centered, confidence level 95 %.

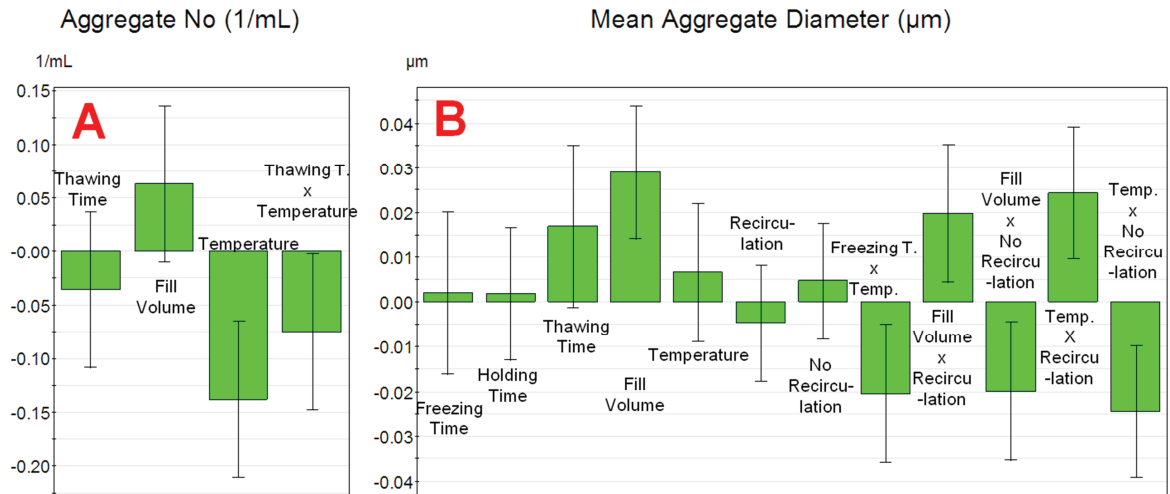


Figure S4: Coefficient plots for aggregation response models derived from DoE-screening; scaled and centered, confidence level 95 %.

## 5 In-Situ Protein Secondary Structure Determination in Ice: Raman Spectroscopy-Based Process Analytical Tool for Frozen Storage of Biopharmaceuticals

Ulrich Roessl,<sup>1,2</sup> Stefan Leitgeb,<sup>1</sup> Sigrid Pieters,<sup>3</sup> Thomas De Beer,<sup>4</sup> Bernd Nidetzky<sup>1,2</sup>

*1 Research Center Pharmaceutical Engineering GmbH, Graz, Austria*

*2 Institute for Biotechnology and Biochemical Engineering, Graz University of Technology, Austria*

*3 Dept. Analytical Chemistry and Pharmaceutical Technology, Free University of Brussels, Belgium*

*4 Laboratory of Pharmaceutical Process Analytical Technology, Ghent University, Belgium*

### **Abstract**

A Raman spectroscopy-based method for in-situ-monitoring of secondary structural composition of proteins during frozen and thawed storage was developed. A set of reference proteins with different  $\alpha$ -helix and  $\beta$ -sheet compositions was used for calibration and validation in a chemometric approach. Reference secondary structures were quantified with circular dichroism (CD) spectroscopy in the liquid state. Partial least squares (PLS) regression models were established which enable estimation of secondary structure content from Raman spectra. Quantitative secondary structure determination in ice was accomplished for the first time and correlation with existing (qualitative) protein structural data from the frozen state was achieved. The method can be used in the presence of common stabilizing agents and is applicable in an industrial freezer setup. Raman spectroscopy represents a powerful, non-invasive, and flexibly applicable tool for protein stability monitoring during frozen storage.

## ***Abbreviations***

ADH: Alcohol dehydrogenase, ANS: 8-anilino-1-naphthalenesulfonic acid, BSA: Bovine serum albumin, CD: Circular dichroism, F/T: Freezing and thawing, HDX-MS: Hydrogen/deuterium exchange mass spectrometry, IR: Infrared, LDH: L-lactic dehydrogenase, PAT: Process analytical technology; PLS: Partial least squares, rhG-CSF: Recombinant human granulocyte-colony stimulating factor, rhIgG: Recombinant human immunoglobulin G, RMSE: Root mean square error.

## **Introduction**

Freezing bulk volumes of pharmaceutical protein solutions is a widely used, yet potentially critical unit operation. Increased shelf life and flexibility in storage and logistics is opposed by the risk of inactivation and aggregation of considerable amounts of high-value protein drugs upon freezing and thawing (F/T).<sup>1</sup> Protein degradation can be triggered by cold denaturation, cryoconcentration of (co-)solutes, and concomitant reduction of solubility as well as by exposure to surfaces of ice crystals or insoluble additives/excipients.<sup>2</sup> Given the large volumes of up to several hundred liters of concentrated protein product stored at industrial scale, any information about protein integrity inside a freeze container is highly desirable and would provide important information for F/T process design. Various analytical methods allow for an assessment of the impact of F/T processing on protein stability, however only in the thawed state at the beginning and the very end of the process.<sup>3-6</sup>

In ice, monitoring of any stability parameter whatsoever was not possible since most established methods for probing protein conformational or colloidal stability require liquid and/or transparent solvents. For infrared (IR) based methods, the contributions of frozen water is the prime factor disturbing structural analysis.<sup>7</sup> However, promising results were obtained by using IR microscopy.<sup>8</sup> Solid state NMR might allow for protein structure assessment in ice, but lacks applicability as process analytical technology (PAT).<sup>9,10</sup> Also, hydrogen/deuterium exchange mass spectrometry (HDX-MS) was used to study conformational changes of proteins in the frozen state.<sup>11,12</sup> The requirement of D<sub>2</sub>O and the slow isotopic exchange at low temperatures renders HDX-MS impractical for broad application in monitoring of protein freezing processes. Fluorescence probes of protein conformation employing 8-anilino-1-naphthalenesulfonic acid (ANS) provided qualitative or semi-quantitative information about protein structural characteristics in the frozen state.<sup>13</sup> However, the presence of an extrinsic fluorophore in pharmaceutical protein formulations can be considered problematic.

Raman spectroscopy is a non-invasive method with broad applicability to biochemical and pharmaceutical problems.<sup>14,15</sup> The extent of the Raman shift is specific for chemical bonds and their vibrational modes. Several regions in the Raman spectrum can be assigned to interactions of the laser light with protein backbone amides. They serve as indicators for the presence of secondary structural elements in proteins. Most important ones are the amide I band (H-bonded C=O stretching) between 1600 and 1700 cm<sup>-1</sup>, amide III band (N-H and C-H bending) at around 1230-1340 cm<sup>-1</sup> and C-C stretching bands at 890-1060 cm<sup>-1</sup>.<sup>16,17</sup> Raman is not disturbed by the presence

of water and ice, and it can be easily applied for process surveillance. Even though Raman has been utilized for qualitative assignment of secondary structural elements in the frozen state,<sup>18</sup> the determination of  $\alpha$ -helix or  $\beta$ -sheet content by in-situ Raman spectroscopy was not demonstrated before.

Herein we show that Raman spectroscopy can be extended to quantitatively estimate secondary protein structure in frozen solutions, and that it can be applied for stability monitoring of pharmaceutical proteins during F/T and frozen storage. For that purpose, relative  $\alpha$ -helix and  $\beta$ -sheet content of 14 proteins were obtained with circular dichroism (CD) spectroscopy in the liquid state. Partial least squares (PLS) regression was then used to establish models for the prediction of  $\alpha$ -helix and  $\beta$ -sheet content from Raman spectra.

## **Materials and Methods**

### Materials

Chicken egg white lysozyme, bovine pancreatic trypsin type I, ribonuclease A and insulin, bovine serum albumin (BSA), bovine milk-derived  $\beta$ -lactoglobulin, porcine gastric mucosa pepsin, rabbit muscle L-lactic dehydrogenase (LDH), *Saccharomyces cerevisiae* alcohol dehydrogenase (ADH) and *Bacillus subtilis*  $\alpha$ -amylase were from Sigma Aldrich, St. Louis, MO, USA. rhG-CSF was kindly provided by Sandoz (Kundl, Austria). IgGs were donations from undisclosed sources. Chemicals and reagents used were from Carl Roth GmbH + Co. KG (Karlsruhe, Germany). Vivaspin ultrafiltration columns from GE Healthcare, Little Chalfont, UK, (MWCO 3 kDa – 10 kDa) were used for buffer exchange and sample concentration.

### Sample preparation

Proteins powders were resuspended in suitable sample buffer (Table 1). Buffer exchange was performed twice, followed by sample concentration. Final protein concentration was determined by UV absorbance (Beckman Coulter DU 800 spectrophotometer). Extinction coefficients for 280 nm were calculated with ExPASy ProtParam,<sup>19</sup> if not provided by the supplier. TRIS-HCl and acetate buffer (10 mM) were chosen to avoid large pH shifts during freezing.<sup>20</sup> In Table 1 protein names and origin, buffer type, pH, and concentrations of analyzed samples are displayed. After completion of CD and Raman measurements in the liquid state, samples were frozen in liquid nitrogen and stored at -20°C over night, until recording of Raman spectra in the frozen state took place.

F/T cycle experiments were performed in a 700 mL stainless steel freeze container by Zeta Biopharma GmbH (Lieboch, Austria) circulated and cooled by an external freeze controller (Tango Nuevo thermostat by Peter Huber Kaeltemaschinenbau GmbH, Offenburg, Germany). Each cycle lasted 4 hours and contained a 2-hour freezing step followed by a 2-hour thawing step. During the freezing step bulk temperatures of -30°C were reached. Thawing was accomplished by increasing thermofluid temperature to 20°C after the freezing step. The Raman probe head, described below, was installed via a specialized container lid with an adapted fitting. The probe head was placed in a way that sampling occurred in a position exactly at half radius of the container and approximately at half of the fill height for 700 mL. The container is equipped with cooling coils mounted in its vertical axis. Thus, high protein concentrations could be expected in half-radial regions due to

macroscopic cryoconcentration.<sup>1</sup> Heat stressing of rhIgG1-A was performed for 10 minutes at 74°C in a volume of 1 mL on a Thermomixer Comfort by Eppendorf, Hamburg, Germany.

**Table 1: Reference proteins used for CD and Raman spectroscopic analysis.**

Protein	Organism	Buffer (10 mM)	pH (20°C)	Concentration (mg/mL)
BSA	<i>Bos tauris</i>	TRIS-HCl	7.5	30/70 <sup>a</sup>
Insulin	<i>Bos tauris</i>	TRIS-HCl	3.0 <sup>b</sup>	36
Muscle LDH	<i>Oryctolagus cuniculus</i>	TRIS-HCl	7.5	22 <sup>c</sup>
rhG-CSF	<i>Homo sapiens</i>	Acetate	4.4	36/60 <sup>a</sup>
Lysozyme	<i>Gallus gallus</i>	TRIS-HCl	7.5	31/62 <sup>a</sup>
ADH	<i>Saccharomyces cerevisiae</i>	TRIS-HCl	8.6	25
$\alpha$ -Amylase	<i>Bacillus subtilis</i>	Acetate	5.0	25/34 <sup>a</sup>
Ribonuclease A	<i>Bos tauris</i>	TRIS-HCl	7.5	30/65 <sup>a</sup>
Pepsin	<i>Sus scrofa</i>	Acetate	4.4	7 <sup>c</sup>
$\beta$ -Lactoglobulin	<i>Bos tauris</i>	Acetate	5.7	30
Trypsin	<i>Bos tauris</i>	TRIS-HCl	7.5	20
rhIgG1-A	<i>Homo sapiens</i>	Acetate	5.7	30/69 <sup>a</sup>
rhIgG1-B	<i>Homo sapiens</i>	Acetate	5.7	26
rhIgG2	<i>Homo sapiens</i>	Acetate	5.7	30/57 <sup>a</sup>

<sup>a</sup> two concentrations of native protein were examined when higher concentrations were reached easily by ultrafiltration.

<sup>b</sup> Sufficiently high concentrations of soluble insulin could only be reached by acidification using HCl.

<sup>c</sup> higher concentrations were not reached using ultrafiltration; Raman spectra from the frozen state could not be analyzed due to insufficient scattering yields.

## CD spectroscopy

CD spectra of liquid samples were recorded with a Jasco J-715 spectropolarimeter (Tokyo, Japan) at room temperature between 190 – 260 nm. A cylindrical cuvette of 10  $\mu$ m path length was used.

The respective protein concentration was as stated in Table 1. Spectra were recorded five times, averaged, and corrected for the appropriate buffer blank. The relative secondary structural composition was calculated using the CDSSTR algorithm implemented at the Dichroweb server.<sup>21</sup>

The resulting fractions for *Helix1* and *Helix2*, *Strand1* and *Strand2*, as well as *Turns* and *Unordered* were each added up to single values for  $\alpha$ -helix,  $\beta$ -sheet and Others, respectively

## Raman spectroscopy

Raman spectra were recorded using a RamanRXN2™ Hybrid Analyzer by Kaiser Optical Systems, Ann Arbor, MI, USA, equipped with a 785 nm laser and a short focusing ¼ inch MR immersion probe head. Spectra were recorded and processed using iC Raman™ software. Raman scattering in the range between 100 and 1890  $\text{cm}^{-1}$  was recorded three times for five seconds and averaged. Unless otherwise mentioned, Raman spectra were acquired in sample volumes of 500-1000  $\mu\text{L}$ , placed in a lightproof box. Corresponding buffer-alone spectra were subtracted prior to any further analysis.

## PLS-Regression Modeling

33 buffer-subtracted Raman spectra were loaded into The Unscrambler™ X software. Detrending, standard normal variate (SNV)-correction and Savitzky-Golay smoothing were performed and a PLS regression model was established with respect to the relative content of  $\alpha$ -helix,  $\beta$ -sheet, and other structures measured with CD. The model was cross-validated (random with 5 segments) using Unscrambler™ X. Based on Raman spectra from frozen samples (frozen buffer signals subtracted) the model was used to predict  $\alpha$ -helix and  $\beta$ -sheet content in frozen protein solutions.

## Results and Discussion

### Reference protein selection

The proteins presented in Table 1 were chosen to provide representative variation in relative secondary structure content, thus allowing the generation of a robust and widely applicable model. Additionally, we applied 3 % (w/v) SDS to (partially) denature the reference proteins and thus further increase structural variation within the set of model proteins.

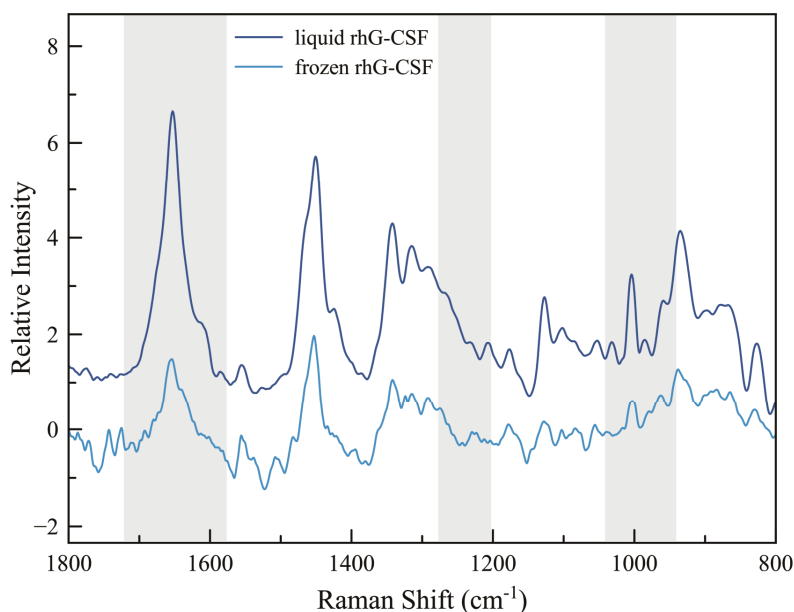


**Figure 1: Buffer subtracted spectra of rhG-CSF in the liquid and the frozen state. Regions considered in the PLS models are highlighted in grey.**

### Sample Preparation

Raman requires concentrated protein solutions, ideally  $>25$  mg/mL. A special CD-cuvette (light path =  $10\ \mu\text{m}$ ) was required to measure CD and Raman from the same sample. The need for dilution would have complicated especially the measurements of SDS-unfolded samples. Conditions for SDS-micelle formation would have changed when keeping molar protein/denaturant ratio constant with dilution.

Besides their applicability in CD measurements, Tris-HCl and acetate buffer (10 mM) were employed as they exhibit only marginal pH shifts upon freezing.<sup>20</sup>

For proteins, which were easily enriched with spin columns, a second, higher concentrated, sample was measured in addition to the ones near the lower concentration limit of about 20-25 mg/mL (see Table 1). Other proteins, such as porcine pepsin, could not be concentrated above that limit. For bovine insulin only acidification to pH 3 allowed for sufficient concentration. Altogether, 33 samples were prepared for corresponding CD- and Raman measurements.

#### Acquisition of CD- and Raman spectra in the liquid state

Results of secondary structure calculations from CD spectra using Dichroweb are summarized in the Supporting Information. Immediately after CD measurements, 33 Raman spectra were recorded from the same liquid preparations. Despite its low concentration (7 mg/mL) characteristic Raman scattering was observed for porcine pepsin.

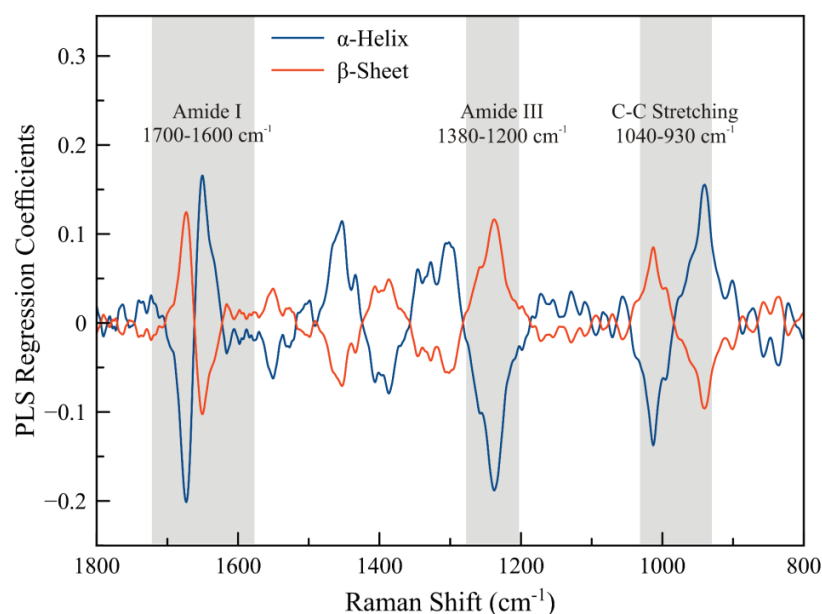


**Figure 2: Regression coefficient plot from the PLS regression model for the Raman spectra. High variations with secondary structure were found in amide I (1700-1600 cm<sup>-1</sup>), amide III (1380-1200 cm<sup>-1</sup>) and C-C-stretching region (1040-930 cm<sup>-1</sup>). Regions considered in the PLS models are highlighted in grey (1720-1580 cm<sup>-1</sup>, 1280-1200 cm<sup>-1</sup> and 1040-930 cm<sup>-1</sup>).**

## Model generation from liquid-state Raman spectra

A first PLS regression analysis was performed from the Raman spectra ranging between 300 to 1890  $\text{cm}^{-1}$ . We found highest coefficients of regression with secondary structural data in the spectral regions between 1600 and 1700  $\text{cm}^{-1}$ , 1200 and 1380  $\text{cm}^{-1}$ , as well as between 930 and 1040  $\text{cm}^{-1}$  (see Figure 2). Those regions exactly correspond to regions known for their specificity for secondary protein structure, namely amide I-, amide III- and the C-C-stretching region. The amide I-band can be assigned to C=O stretching vibrations with small contributions from the C-N stretching and the N-H in-plane bending. Amide III bands arise from in-phase combination of N-H in-plane bending and C-N stretching.<sup>23</sup> PLS regression showed highly positive correlations with  $\alpha$ -helix content at 1650-1660  $\text{cm}^{-1}$  and 890-945  $\text{cm}^{-1}$ . At 1670-1680  $\text{cm}^{-1}$  and also at around 1210-1250  $\text{cm}^{-1}$ , positive correlation with  $\beta$ -sheet content was maximal. This was in agreement with literature on protein secondary structure investigations using Raman spectroscopy.<sup>16,17,23</sup> Also, certain regions between 1380 and 1500  $\text{cm}^{-1}$  appeared to correlate with the presence of secondary structure elements and might be assigned to the amide II-band. However, SDS as well as other additives (see Figure 6) showed Raman scattering in this region and hence it was not considered for further model development. Instead, we narrowed the analyzed region in such a way that any SDS contribution could be ruled out. A second PLS regression analysis was performed with respect to the spectral regions 1580-1720  $\text{cm}^{-1}$ , 1200-1280  $\text{cm}^{-1}$  and 930-1040  $\text{cm}^{-1}$  (Figure 2).

The resulting PLS model showed that  $\alpha$ -helix and  $\beta$ -sheet content were predictable from the Raman spectra (Table 2). With coefficients of determination of  $R^2 = 0.82$  for  $\alpha$ -helix and  $R^2 = 0.79$  for  $\beta$ -sheet useable calibrations were achieved.<sup>24,25</sup> Deviations from the predictions can be estimated with the root mean square error (RMSE), which lies at 6.96 % for  $\alpha$ -helix and 4.90 % for  $\beta$ -sheet. Internal cross-validation delivered almost equivalent values. Two PLS-factors were used for the predictions. Figure 3 displays the score plots for  $\alpha$ -helix and  $\beta$ -sheet models reflecting the power of the models to discriminate different compositions of secondary structure. Results from random cross validation using Unscrambler<sup>TM</sup> X are also shown in Table 2.

**Table 2: Performance of PLS regression models.  $R^2$ : Coefficient of determination; RMSE: Root mean square error**

	$\alpha$ -Helix		$\beta$ -Sheet	
	$R^2$	RMSE (%)	$R^2$	RMSE (%)
Calibration	0.82	6.96	0.79	4.90
Cross-Validation	0.79	8.00	0.72	5.73

### Assessment of secondary structure of reference proteins in ice

After CD- and Raman spectroscopy of 33 reference protein samples in the liquid state, the investigated preparations were frozen and Raman spectra were collected in the frozen state. The presence of ice was checked by examination of the ice peak at  $215\text{ cm}^{-1}$ .<sup>22</sup> Like in the liquid state, three acquisitions, five seconds each, were averaged. Longer acquisition times would have increased scattering intensities and thereby reduced noise. However, exposure to the intensive laser beam had to be limited. Longer exposure times would have led to sample melting during the measurements. Buffer subtracted Raman spectra of liquid and frozen rhG-CSF are shown as examples in Figure 1. As can be seen there, deviations were minimal in the spectral regions between  $930$  and  $1720\text{ cm}^{-1}$ . Apart from the overall lower scattering intensities we found no influence of sample freezing on Raman spectra of any sample. Pepsin and LDH were the only reference proteins for which scattering intensities after buffer signal subtraction were too low to allow for consistent predictions from the frozen state. For the other proteins, the established models could be applied.

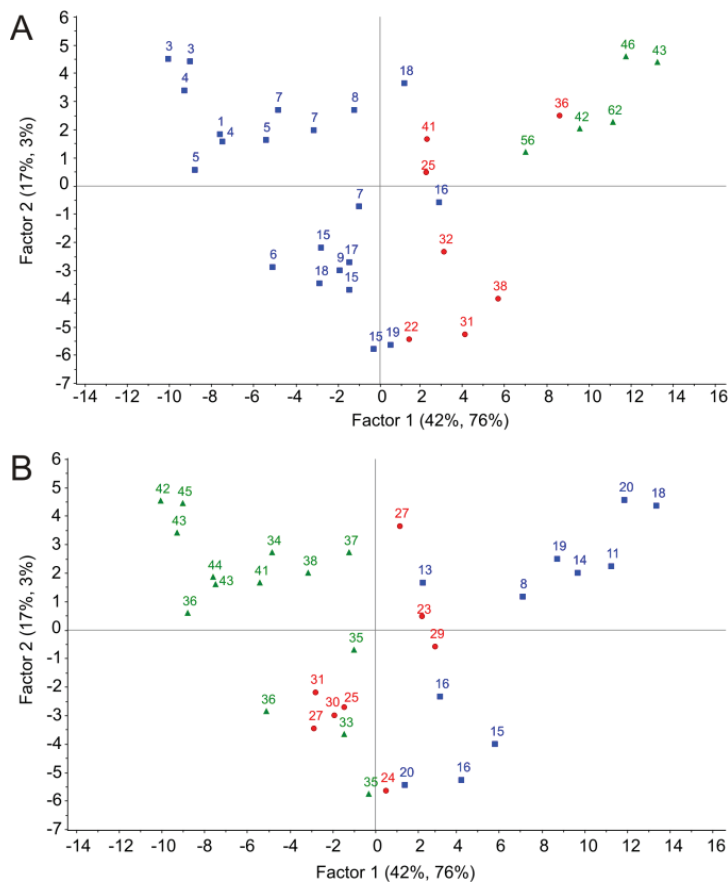


**Figure 3: Score plots of the PLS regression models for  $\alpha$ -helix (A) and  $\beta$ -sheets (B). Color coding and labels represent relative content of the respective secondary structural element.**

Figure 4 displays the secondary structure predictions from frozen state Raman measurements of the native reference proteins, compared with CD results from the liquid state. Many proteins showed increment of  $\alpha$ -helix content upon freezing, while some showed no difference or a loss.  $\beta$ -sheet content was reduced by freezing in most of the proteins. But in some cases, also an increase or no change was found. Considering also the SDS-unfolded samples, we found no indication that sample freezing could influence Raman spectra per se. Predicted values for all frozen reference proteins can be taken from the Supporting Information.

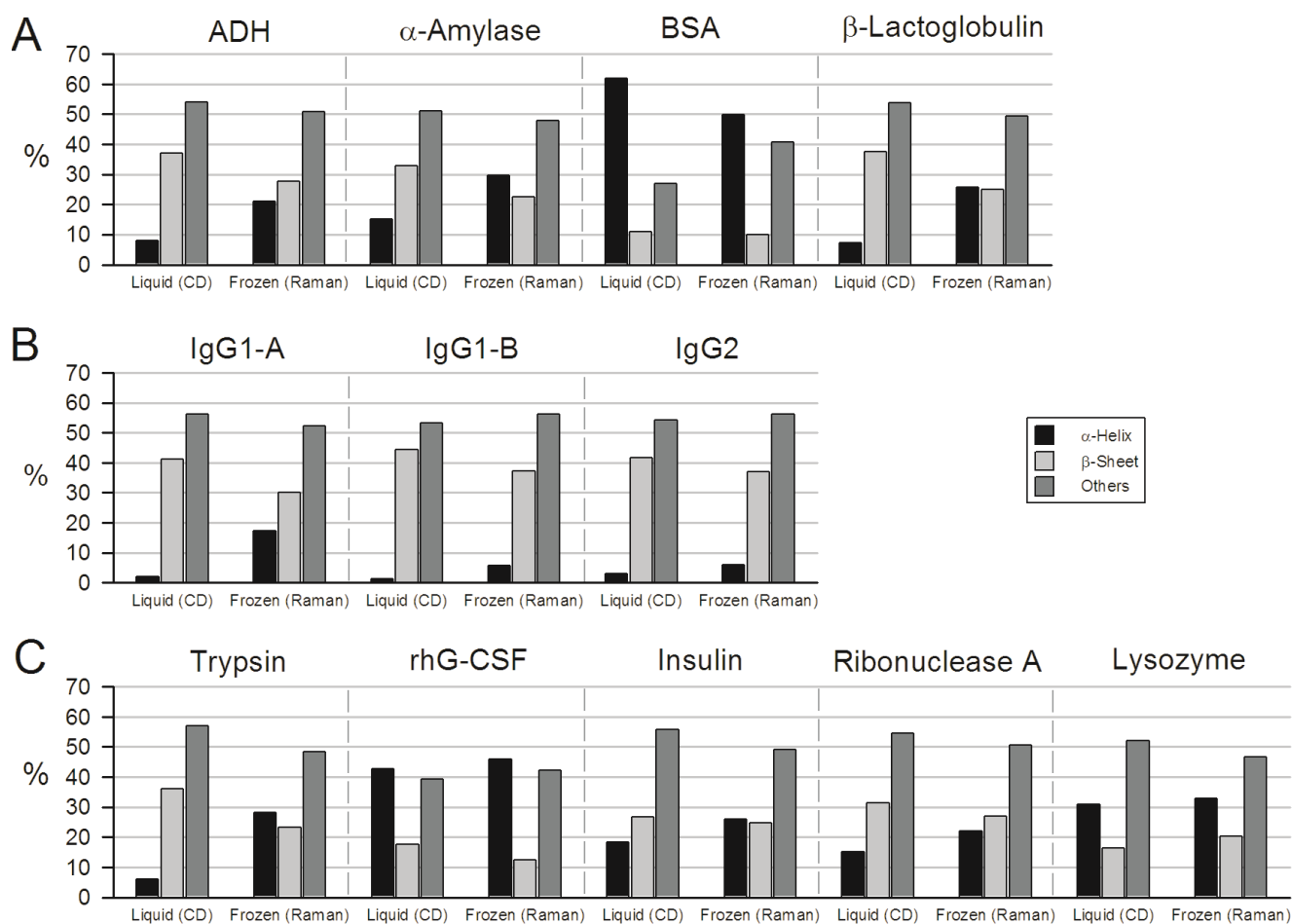


**Figure 4: Relative content of secondary structural elements in liquid state (CD) and frozen state (Raman); A: proteins for which unfolding in ice could be confirmed and quantified on secondary structural level using Raman. B: Monoclonal antibodies. C: Other reference proteins.**

## Detection of protein denaturation in ice

ADH,  $\alpha$ -Amylase, BSA, and  $\beta$ -Lactoglobulin exhibited pronounced structural differences in the liquid and the frozen state (Figure 4A). For these proteins, unfolding in ice has been demonstrated before by using an ANS-fluorescence method.<sup>26</sup> With frozen state Raman spectroscopy, we were able not only to confirm unfolding of these proteins in ice, but even to assign a degree of unfolding by determination of changes in secondary structure. ADH,  $\alpha$ -amylase, and  $\beta$ -lactoglobulin showed pronounced increases in  $\alpha$ -helical content and decreases of  $\beta$ -sheets and other structures in the frozen state. Frozen BSA exhibited fewer  $\alpha$ -helical structures and an increase of other structures while  $\beta$ -sheet content remained unchanged.

Three monoclonal antibodies (IgG) were investigated in our study. All exhibited an increase in  $\alpha$ -helix content and a decrease of  $\beta$ -sheet content in the frozen state (Figure 4B). Subtle conformational changes in ice were reported for an IgG before using infrared microscopy of partially frozen samples.<sup>8</sup>

For other reference proteins, evidence for unfolding in the frozen state was not found in literature. However, for trypsin we detected considerable structural changes in ice. Largely unaltered secondary structures in the frozen state were found for rhG-CSF, ribonuclease A, lysozyme, and acid-unfolded insulin (Figure 4C).

## Secondary structure monitoring during F/T

We conducted repeated F/T cycle experiments with IgG1-A inside a 700 mL stainless steel freeze container in order to demonstrate the method's applicability as PAT tool for monitoring protein stability during F/T processes. Ten F/T cycles were performed (4 hours each) and Raman spectra were recorded in the absence and the presence of 7% trehalose which is known for stabilizing proteins during F/T. Without trehalose, there was no structural change during the first F/T cycle (Figure 5A). Starting with the second cycle we observed secondary structure changes in the frozen state (Figure 5B). Upon thawing, a native-like structure was reassumed. This behavior was observed throughout ten F/T cycles.

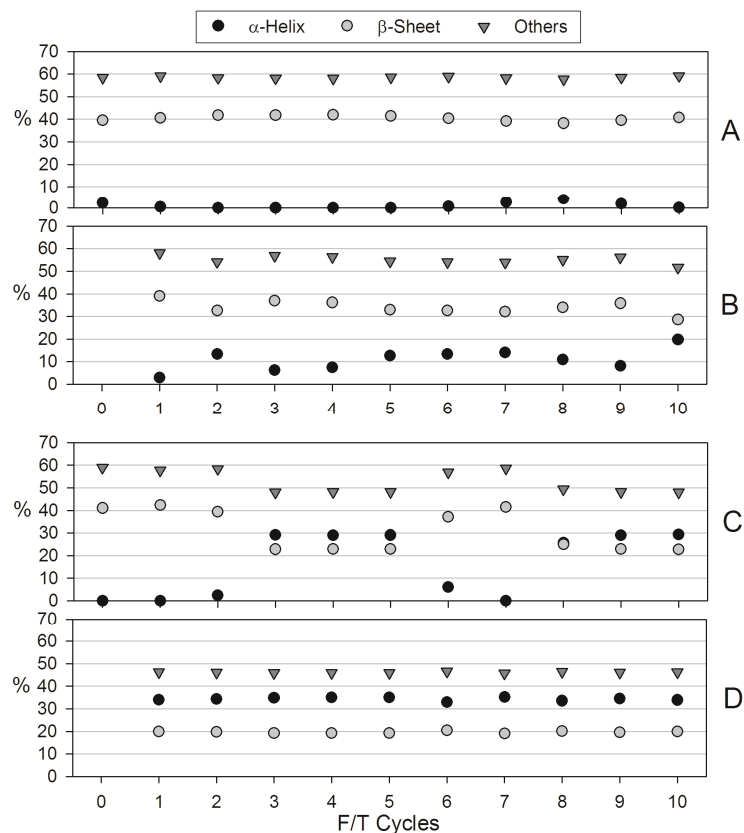


**Figure 5: Monitoring secondary structure of IgG1-A during F/T (25 mM citrate buffer, pH 6.5). A: IgG1-A in the liquid/thawed state (20°C); B: IgG1-A in the frozen state (-30°C); C: IgG1-A with 7% trehalose in the liquid/thawed state (20°C); D: IgG1-A with 7% trehalose in the liquid/thawed state (-30°C).**

The addition of 7% trehalose did not entail F/T stabilization of the antibody. From the first F/T cycle on, considerable unfolding was detected in the frozen state (Figure 5D). Only up to the 3<sup>rd</sup> cycle, refolding to native-like structure after thawing was observed (Figure 5C). During cycle 6 and 7 temporary recovery to native-like structure was noticed, but native structure was lost again in the following runs.

The instability of IgG1-A might be explained with trehalose crystallization in the frozen state promoting protein unfolding by increased surface exposure.<sup>27</sup> However, examination of characteristic bands at 1050, 1100, 1120, 1330, and 1350 cm<sup>-1</sup> did not indicate presence of crystalline trehalose.<sup>28</sup> Yet, the addition of trehalose did not improve conformational stability of IgG1-A.

The presence of trehalose itself does not disturb Raman analysis. Minor contributions are found in the regions between amide I and amide III regions (Figure 6) and are not considered in the PLS model. To test whether common freeze stabilizers interfere with the presented method we recorded spectra in the presence of trehalose (3 % / 7 % w/v) , sucrose, mannitol (3 % w/v each) and Tween<sup>TM</sup> 80 (0.02% w/v) (Figure 6). Here, the total volume was 1 mL. In the liquid state, there was practically no difference between the spectra with different additives. In the frozen state, higher discrepancies between the samples, especially for  $\alpha$ -helices, were predicted from Raman spectra (see Supporting Information). Most likely, this might be due to different protein conformational stabilities in the presence of the different additives.

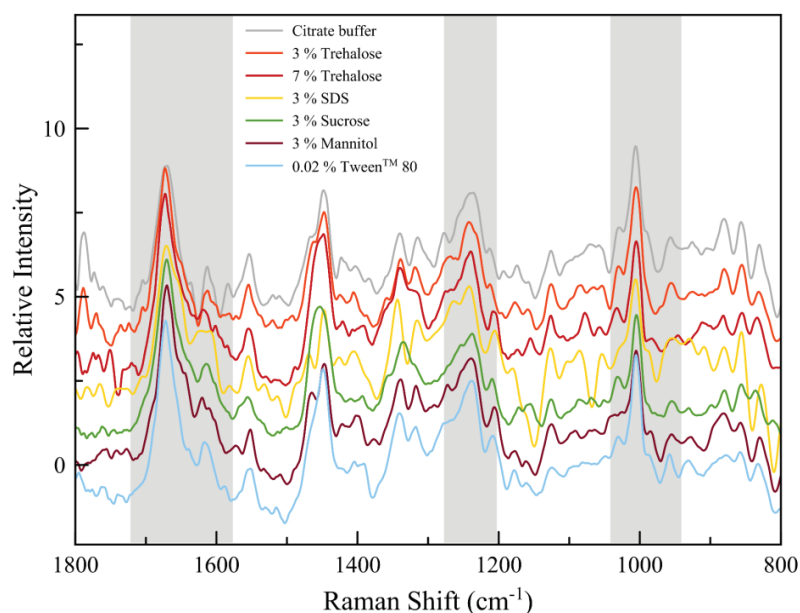


**Figure 6: Raman spectra of liquid IgG1-A (30 mg/mL) in the presence of various additives; Regions considered in the PLS models are highlighted in grey.**

#### Distinguishing native-like and non-native IgG1 structures

For IgG1 it was shown before that F/T cycles induce the formation of aggregates exhibiting native-like structure. Thermal stressing leads to non-native aggregation with an increase of  $\alpha$ -helix content and a loss of  $\beta$ -sheet structures.<sup>29,30</sup> These results were confirmed here using liquid state Raman, and the same trends were also seen in frozen samples. In liquid samples no difference between unstressed and F/T stressed samples were observed, while unstressed samples exposed to 74°C for

10 minutes exhibited higher  $\alpha$ -helix- and lower  $\beta$ -sheet content (see Supporting Information). In the frozen state, as shown above, IgG1-A showed already elevated  $\alpha$ -helix content and reduced  $\beta$ -sheet content. Heat stressed samples exhibited even higher amounts of  $\alpha$ -helices and lower  $\beta$ -sheet content in the frozen state. In addition, samples were centrifuged and reconstituted with a minimal amount of buffer (25 mM citrate, pH 6.5). This served to increase relative aggregate content and the contribution of the aggregates to the Raman signal. Again, in the liquid and the frozen state, we found native-like structures for F/T stressed samples as well as lower contents of  $\beta$ -sheets and higher amounts of  $\alpha$ -helices in heated samples. Thus, with our method we were able to confirm native aggregation of IgG1-A upon F/T and non-native aggregation after heat exposure.

#### Potential method limitations

Evidence presented in this work shows that Raman is a very useful and convenient technique for protein stability monitoring during F/T and frozen storage. However, some aspects shall be mentioned here that should be considered for its application. One potential limitation of Raman spectroscopy from frozen samples is the heat generation by the strong focused laser beam. Long-lasting exposure increases the risk of sample melting. In experiments which were performed on samples at mL-scale we avoided melting by reduction of exposure time to a minimum. The low scattering yields obtained with Raman in turn increases the noise at very short acquisition times. This difficulty could be overcome with the use of specialized non-focusing probe optics.

Also, a reduction of laser power together with an increase of acquisition time might bear advantages for measuring small or poorly cooled samples. However, at larger scales and especially when applied inside a freeze container heat transfer from the inspected spot is faster and melting won't need to be expected.

Subtraction of buffer spectra from the protein's Raman spectra conveniently served to reduce background contributions and thereby rendered PLS-model generation possible. In blanks accurate mimicry of sample conditions regarding temperature, phase state, and co-solutes is hence necessary. The relatively high protein concentrations of at least 25 mg/mL required for Raman scattering can be regarded as only a minor limitation. Proteins are usually frozen at higher concentrations since they are more stable when they are stored this way.<sup>1</sup>

We used our method for secondary structure assessment of an IgG1 in the presence of trehalose, sucrose, mannitol, Tween™ 80 and SDS. Other excipients with higher Raman scattering yields would be more prone to interfere with our method, and their compatibility would have to be evaluated thoroughly before application.

With regard to the pilot-scale monitoring experiments it should be noted that only a small fraction of the total container volume could be inspected with the used Raman optic. With a focal spot size of 50  $\mu\text{m}$  and a focal plane virtually at the probe window, the illuminated volume can be estimated to be no larger than 200  $\mu\text{L}$ . With respect to the inhomogeneous distribution of solutes in frozen bulk solutions, variation of the sampling position should be considered for further process analytic applications of that method.

The significance of a conformational change observed for a specific protein in the frozen state, as well as its actual impact on the protein's stability needs to be evaluated for each protein individually. Unfolding in ice might not inevitably lead to aggregation or activity loss. But examination of folding states in ice would certainly widen our capabilities for studying and improving frozen storage conditions. We are certain that opportunities arising with in-situ Raman spectroscopy of frozen protein samples clearly outweigh potential limitations of this innovation.

## ***Conclusions***

We demonstrated that Raman spectroscopy represents a powerful method for determination of secondary protein structure directly in the frozen state. We accomplished the development of the method into a flexibly applicable tool of process analytical technology for F/T operations. The occurrence of partial unfolding of proteins in ice is demonstrated at a quantitative secondary structural level for the first time. It is also shown that such unfolding events can be reversible or irreversible upon thawing. The method provides unprecedented opportunities for in-depth systematic examination of F/T operations in research and development, and supports design and optimization of F/T processes at manufacturing scale.

Implications of this work in the field of pharmaceutical protein technology are broad. With the method presented, researchers and producers will have access to nearly real-time information about protein stability at any time during frozen storage. This will significantly facilitate process characterization, optimization and qualification. It will increase flexibility and lead to faster generation of results from stability testing. Early recognition of stability issues could massively save cost and development time. As various probe sizes and technologies are available adaptation to specific demands facilitates convenient and robust process surveillance. Due to its flexibility and potential applicability to any other frozen protein, the outlined method represents a major innovation in biopharmaceutical process analytical technology and will contribute to ongoing consolidation of Quality by Design principles in biopharmaceutical industry.

## ***Acknowledgments***

For providing Raman instrumentation and for technical support the authors thank Kaiser Optical Systems and Carsten Uerpmann. Special thanks for financial support and an excellent collaboration go to Zeta Biopharma. We also thank Patrick Wahl from Research Center Pharmaceutical Engineering for his assistance. Furthermore, for continuous help and advice we want to thank Satish Singh, Pfizer Inc.

This work has been funded within the Austrian COMET program under the auspices of the Austrian Federal Ministry of Transport, Innovation and Technology (bmvit), the Austrian Federal Ministry of Economy, Family and Youth (bmwfj), and the State of Styria (Styrian Funding Agency SFG). COMET is managed by the Austrian Research Promotion Agency FFG.

## References

1. Singh SK, Nema S. 2010. Freezing and thawing of protein solutions. In *Formulation and process development strategies for manufacturing biopharmaceuticals*; Jameel F, Hershenson S, Eds. Hoboken, New Jersey: JohnWiley & Sons, pp 625–675.
2. Singh S, Kolhe P, Wang W, Nema S. 2009. Large-scale freezing of biologics; A practitioner's review. Part one: Fundamental aspects. *Bioprocess Int* 7:32–44.
3. Berkowitz SA, Engen JR, Mazzeo JR, Jones GB. 2012. Analytical tools for characterizing biopharmaceuticals and the implications for biosimilars. *Nat Rev Drug Discov* 11(7):527–540.
4. Pelton JT, McLean LR. 2000. Spectroscopic methods for analysis of protein secondary structure. *Anal Biochem* 277:167–176.
5. Manning MC, Patel K, Borchardt RT. 1989. Stability of protein pharmaceuticals. *Pharm Res* 6:903–918.
6. Manning MC, Chou DK, Murphy BM, Payne RW, Katayama DS. 2010. Stability of protein pharmaceuticals: An update. *Pharm Res* 27:544–575.
7. Pieters S, Vander Heyden Y, Roger J-M, D'Hondt M, Hansen L, Palagos B, De Spiegeleer B, Remon J-P, Vervaet C, De Beer T. 2013. Raman spectroscopy and multivariate analysis for the rapid discrimination between native-like and non-native states in freeze-dried protein formulations. *Eur J Pharm Biopharm* 85:263–271
8. Schwegman JJ, Carpenter JF. 2009. Evidence of partial unfolding of proteins at the ice/freezing-concentrate interface by infrared microscopy. *J Pharm Sci* 98:3239–3246.
9. Havlin RH, Tycko R. 2005. Probing site-specific conformational distributions in protein folding with solid-state NMR. *Proc Natl Acad Sci USA* 102:3284–3289.
10. Siemer A, Huang K, McDermott AE. 2010. Protein–ice interaction of an antifreeze protein observed with solid-state NMR. *Proc Natl Acad Sci* 107:17580–17585.
11. Zhang A, Qi W, Singh S, Fernandez E. 2011. A new approach to explore the impact of freeze-thaw cycling on protein structure: Hydrogen/deuterium exchange mass spectrometry (HX-MS). *Pharm Res* 28:1–15.
12. Zhang A, Singh SK, Shirts MR, Kumar S, Fernandez EJ. 2012. Distinct aggregation mechanisms of monoclonal antibody under thermal and freeze-thaw stresses revealed by hydrogen exchange. *Pharm Res* 29:236–250.
13. Gabellieri E, Strambini GB. 2003. Perturbation of protein tertiary structure in frozen solutions revealed by 1-anilino-8-naphthalene sulfonate fluorescence. *Biophys J* 85:3214–3220.
14. Wen Z. 2007. Raman spectroscopy of protein pharmaceuticals. *J Pharm Sci* 96:2861–2878.

15. Herrero AM. 2008. Raman spectroscopy a promising technique for quality assessment of meat and fish: A review. *Food Chem* 107:1642–1651.
16. Herrero AM, Carmona P, Jimenez-Colmenero F, Ruiz-Capillas C. 2010. Applications of vibrational spectroscopy to study protein structural changes in muscle and meat batter systems. In *Handbook of vibrational spectroscopy*; Chalmers JM, Griffiths PR, Eds. Hoboken, New Jersey: JohnWiley & Sons, pp 315–328..
17. Tantipolphan R, Rades T, Medlicott NJ. 2008. Insights into the structure of protein by vibrational spectroscopy. *Curr Pharm Anal* 4:53–68.
18. Dong J, Hubel A, Bischof JC, Aksan A. 2009. Freezing-induced phase separation and spatial microheterogeneity in protein solutions. *J Phys Chem B* 113:10081–10087.
19. Gasteiger E, Hoogland C, Gattiker A, Duvaud S, Wilkins MR, Appel RD, Bairoch A. 2005. Protein identification and analysis tools on the ExPASy server. In *The proteomics protocols handbook*; Walker JM, Ed. Totowa, New Jersey: Humana Press, pp 571–607.
20. Kolhe P, Amend E, Singh SK. 2009. Impact of freezing on pH of buffered solutions and consequences for monoclonal antibody aggregation. *Biotechnol Prog* 26:727–733.
21. Whitmore L, Wallace BA. 2008. Protein secondary structure analyses from circular dichroism spectroscopy: Methods and reference databases. *Biopolymers* 89:392–400.
22. De Beer TRM, Allesø M, Goethals F, Coppens a, Heyden Y Vander, De Diego HL, Rantanen J, Verpoort F, Vervaet C, Remon JP, Baeyens WRG. 2007. Implementation of a process analytical technology system in a freeze-drying process using Raman spectroscopy for in-line process monitoring. *Anal Chem* 79:7992–8003.
23. Hédoux A, Paccou L, Achir S, Guinet Y. 2012. In situ monitoring of proteins during lyophilization using micro-Raman spectroscopy: A description of structural changes. *J Pharm Sci* 101:2316–2326.
24. Williams P. *Near-infrared technology: Getting the best out of light: a short course in the practical implementation of near-infrared spectroscopy for the user*. PDK Projects, Incorporated.
25. Massart DL, Vandeginste BGM, Buydens LMC, De Jong S, Lewi PJ, Smeyers-Verbeke J, Mann CK. 1998. *Handbook of chemometrics and qualimetrics: Part B*. Amsterdam: Elsevier Science.
26. Gabellieri E, Strambini GB. 2006. ANS fluorescence detects widespread perturbations of protein tertiary structure in ice. *Biophys J* 90:3239–3245.
27. Singh SK, Kolhe P, Mehta AP, Chico SC, Lary AL, Huang M. 2011. Frozen state storage instability of a monoclonal antibody: Aggregation as a consequence of trehalose crystallization and protein unfolding. *Pharm Res* 28:873–885.
28. Connolly B, Patapoff TW, Wang YJ, Moore JM, Kamerzell TJ. 2010. Vibrational spectroscopy and chemometrics to characterize and quantitate trehalose crystallization. *Anal Biochem* 399:48–57.

29. Hawe A, Kasper JC, Friess W, Jiskoot W. 2009. Structural properties of monoclonal antibody aggregates induced by freeze-thawing and thermal stress. *Eur J Pharm Sci* 38:79–87.
30. Vermeer AWP, Norde W. 2000. The thermal stability of immunoglobulin: unfolding and aggregation of a multi-domain protein. *Biophys J* 78:394–404.

## Supporting Information

**Table S1: Secondary structure content of reference proteins determined by CD spectroscopy followed by spectral deconvolution using Dichroweb**

Protein	3 % SDS (w/v)	$\alpha$ -Helix (%)	$\beta$ -Sheet (%)	Others (%)	Concentration (mg/mL)
ADH	+	25	23	53	25
ADH	-	8	37	54	25
$\alpha$ -Amylase	+	15	35	50	25
$\alpha$ -Amylase	-	15	33	51	34
$\beta$ -Lactoglobulin	-	7	38	54	30
$\beta$ -Lactoglobulin	+	56	8	35	30
BSA	-	62	11	27	30
BSA	+	36	19	46	52
BSA	-	46	20	35	70
Insulin	-	18	27	56	36
Insulin	+	41	13	47	27
LDH	+	38	15	47	16
LDH	-	32	16	52	22
Lysozyme	+	22	20	58	31
Lysozyme	-	31	16	52	31
Lysozyme	-	16	29	56	62
Pepsin	+	18	27	56	6
Pepsin	-	19	24	57	7
rhG-CSF	+	42	14	44	25
rhG-CSF	-	43	18	39	60
rhIgG1-A	-	4	43	52	30
rhIgG1-A	-	4	43	52	69
rhIgG1-A	+	7	34	58	30
rhIgG1-B	+	7	35	57	19
rhIgG1-B	-	1	44	53	26
rhIgG2	-	3	45	51	30
rhIgG2	-	3	42	54	57
rhIgG2	+	5	36	57	30
Ribonuclease A	-	15	31	55	30
Ribonuclease A	+	17	25	58	49
Ribonuclease A	-	5	41	54	65
Trypsin	+	9	30	61	20
Trypsin	-	6	36	57	20

**Table S2: Secondary structure content of reference proteins predicted from frozen state Raman spectra**

Protein	3 % SDS (w/v)	$\alpha$ -Helix (%)	$\beta$ -Sheet (%)	Others (%)	Concentration (mg/mL)
ADH	+	33	20	47	25
ADH	-	21	28	51	25
$\alpha$ -Amylase	+	29	23	48	25
$\alpha$ -Amylase	-	30	23	48	34
$\beta$ -Lactoglobulin	-	26	25	49	30
$\beta$ -Lactoglobulin	+	33	20	46	30
BSA	-	50	10	40	30
BSA	+	39	17	44	52
BSA	-	48	11	41	70
Insulin	-	26	25	49	36
Insulin	+	29	23	48	27
Lysozyme	+	29	23	48	31
Lysozyme	-	33	20	47	31
Lysozyme	-	31	21	47	62
rhG-CSF	+	39	17	44	25
rhG-CSF	-	46	12	42	60
rhlgG1-A	-	14	32	54	30
rhlgG1-A	-	2	40	59	69
rhlgG1-A	+	24	26	50	30
rhlgG1-B	+	24	26	50	19
rhlgG1-B	-	6	37	57	26
rhlgG2	-	6	37	57	30
rhlgG2	-	9	35	56	57
rhlgG2	+	21	28	51	30
Ribonuclease A	-	22	27	51	30
Ribonuclease A	+	19	29	52	49
Ribonuclease A	-	15	31	53	65
Trypsin	+	28	23	48	20
Trypsin	-	28	23	48	20

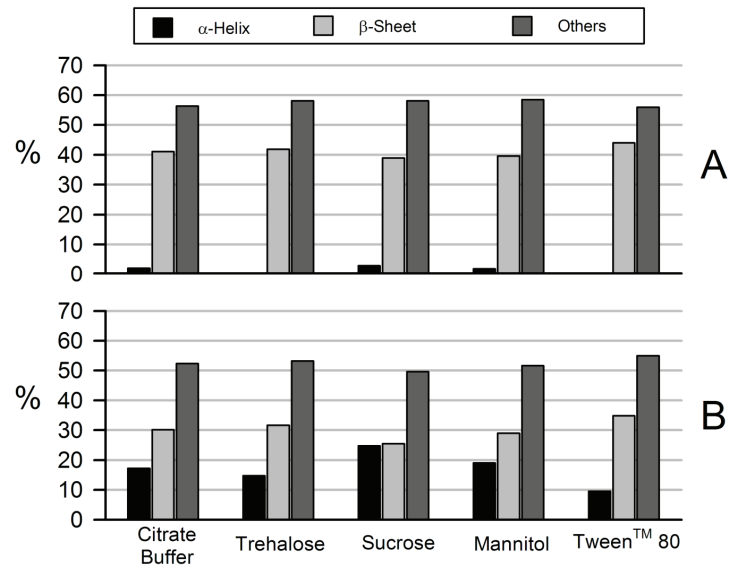


**Figure S1: Secondary structure of IgG1 in the absence and the presence of common stabilizing agents measured with Raman and PLS regression model prediction. A: liquid samples; B: frozen samples.**

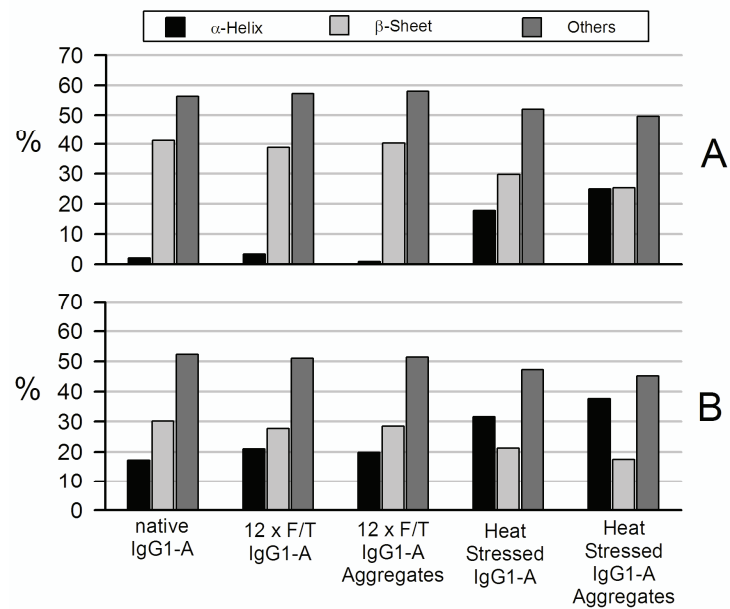


**Figure S2: Impact of F/T and heat stress on IgG1-A conformation in the liquid state (A) and the frozen state (B). Aggregates were washed and enriched by centrifugation and resuspension in sample buffer (25 mM citrate, pH 6.5).**